This is the peer reviewed author accepted manuscript (post print) version of a published work that appeared in final form in:

Xu, Sheng, Wu, Linlong, Doançay, Kutluyl, Alaee-Kerahroodi, Mohammad 2022 'A hybrid approach to optimal TOA-sensor placement with fixed shared sensors for simultaneous multi-target localization', IEEE Transactions on Signal Processing, vol. 70, pp. 1197-1212

This un-copyedited output may not exactly replicate the final published authoritative version for which the publisher owns copyright. It is not the copy of record. This output may be used for non-commercial purposes.

The final definitive published version (version of record) is available at:
https://doi.org/10.1109/TSP.2022.3152232

Persistent link to the UniSA Research Outputs Repository:
https://researchoutputs.unisa.edu.au/11541.2/30189

General Rights

Copyright and moral rights for the publications made accessible in the UniSA Research Outputs Repository are retained by the authors and/or other copyright owners and it is a condition of accessing publications that users recognize and abide by the legal requirements associated with these rights.

- Users may download and print one copy for the purpose of private study or research.
- You may not further distribute the material or use it for any profit-making activity or commercial gain
- You may freely distribute the persistent link identifying the publication in the UniSA Research Outputs Repository

If you believe that this document breaches copyright, please contact us and provide details. We will remove access to the work immediately and investigate your claim.

A Hybrid Approach to Optimal TOA-Sensor Placement with Fixed Shared Sensors for Simultaneous Multi-Target Localization

Sheng Xu, *Member IEEE,* Linlong Wu, *Member IEEE,* Kutluyıl Doğançay, *Senior Member IEEE,* and Mohammad Alaee-Kerahroodi, *Member IEEE*

***Abstract*—This paper focuses on optimal time-of-arrival (TOA) sensor placement for multiple target localization simultaneously. In previous work, different solutions only using non-shared sensors to localize multiple targets have been developed. Those methods localize different targets one-by-one or use a large number of mobile sensors with many limitations, such as low effectiveness and high network complexity. In this paper, firstly, a novel optimization model for multi-target localization incorporating shared sensors is formulated. Secondly, the systematic theoretical results of the optimal sensor placement are derived and concluded using the A-optimality criterion, i.e., minimizing the trace of the inverse Fisher information matrix (FIM), based on rigorous geometrical derivations. The reachable optimal trace of Cramér-Rao lower bound (CRLB) is also derived. It can provide optimal conditions for many cases and even closed form solutions for some special cases. Thirdly, a novel numerical optimization algorithm to quickly find and calculate the (sub-)optimal placement and achievable lower bound is explored, when the model becomes complicated with more practical constraints. Then, a hybrid method for solving the most general situation, integrating both the analytical and numerical solutions, is proposed. Finally, the correctness and effectiveness of the proposed theoretical and mathematical methods are demonstrated by several simulation examples.**

***Index Terms*—Time-of-arrival (TOA), multiple targets simultaneous localization, shared sensors, Cramér-Rao lower bound (CRLB), optimal sensor placement.**

I. Introduction

TARGET localization has always been a key function of many wireless sensing networks and applied successfully in many military and civilian applications, e.g., radar detection, rescue missions and robot navigation [1],[2],[3] [4]. Considering the diversity of the deployed sensors (e.g. radar, sonar, microphone and hydrophone, etc.), there are several types of measurements, e.g., angle-of-arrival (AOA) [5], time-of-arrival (TOA) [6], received-signal-strength (RSS) [7], which are used to estimate the target state [8]. Among these approaches, the circular-TOA target localization has been widely used and attracted a lot of research interests because of its advantages [9] [10]. It is well known that the localization performance is strongly related to the choice of the estimation algorithm. There are many estimators such as extended Kalman filter (EKF), pseudolinear estimator (PLE), pseudolinear Kalman filter (PLKF), maximum-likelihood-estimator (MLE) and particle filter (PF) [11] [12] [13] [14] [15] [16], which can all be applied with different ameliorated performance. However, apart from the estimation algorithms, the localization accuracy also depends on the sensor-target geometry, which has been proven in many works [17] [18] [6] [19]. Specifically, the mean squared error (MSE) of the estimation is a function of the associated sensor-target geometry. Therefore, a deliberate placement of the sensors is highly desired in order to improve the localization accuracy. Especially in some dynamic sensing scenarios where some mobile sensors are deployed, the localization or tracking performance can be optimized by leveraging on the mobility of these sensors [6] [19] [20].

In the last decade, many studies have focused on the optimal TOA sensor placement for single target localization in both the 2-dimensional (2D) and 3-dimensional (3D) cases. The Cramér-Rao lower bound (CRLB) and Fisher information matrix (FIM) are commonly used as the evaluation standards for estimation performance [17] [18]. Meanwhile, some significant optimality criteria including E-optimality criterion (minimizing the maximum eigenvalue of inverse FIM), D-optimality criterion (maximizing the determinant of FIM) and A-optimality criterion (minimizing the trace of inverse FIM), were proposed in [21] to help calculate the optimal sensor-target geometries and achieve the optimal estimation performance. In [22], an optimal sensor placement strategy for range-only (same as the TOA), bearings-only and received-signal-strength localization was developed and the D-optimality criterion was used. An optimal geometry analysis for the elliptic-TOA localization was presented using the A-optimality criterion in [23], when the measurement noise variances of the different sensors are uniform. In [20], the D-optimality criterion was applied to derive a general optimal placement for the optimal sensor configurations with uniform noise variance for single target localization. The

Manuscript received 30th September 2021. The work of Sheng Xu is supported by National Natural Science Foundation of China (61803363) and Guangdong Basic and Applied Basic Research Foundation (2020B1515120054). The work of Linlong Wu and Mohammad Alaee-Kerahroodi is supported in part by ERC AGNOSTIC under grant ID 742648 and in part by FNR CORE SPRINGER under grant C18/IS/12734677. *Corresponding author: Linlong Wu.*

S. Xu is with Guangdong Provincial Key Lab of Robotics and Intelligent System, Guangdong-Hong Kong-Macao Joint Laboratory of Human-Machine Intelligence-Synergy Systems, Shenzhen Institute of Advanced Technology, Chinese Academy of Sciences, Shenzhen, 518055, China. Email: sheng.xu@siat.ac.cn.

K. Doğançay is with UniSA STEM, University of South Australia, Mawson Lakes, 5095, Australia. Email: kutluyil.dogancay@unisa.edu.au.

L. Wu and M. Alaee-Kerahroodi are with the Interdisciplinary Centre for Security, Reliability and Trust (SnT), University of Luxembourg, Luxembourg City L-1855, Luxembourg. Email: linlong.wu, mohammad.alaee@uni.lu.

optimal sensor placement for 2D elliptic-TOA localization using one transmitter and multiple receivers was proposed in [6]. Then, the works of [20], [24] and [6] were improved and extended into the 3D case in [19] for optimal sensor placement. However, these works were all limited to the single target case, whereas in this paper we focus on formulating the localization problem for multiple simultaneous targets, and then find some new results.

For simultaneous multi-target localization, the optimization problem formulation and solution become extremely complex caused by the combination of FIMs for multiple targets. This challenging topic has become very popular recently, since the optimal solution can improve localization performance significantly for different practical applications. In [25], an optimal range-based sensor-target solution was firstly derived for multi-target localization. The convex combination of FIMs for multiple targets was derived and analyzed. The optimization problem was solved by a proposed gradient-based algorithm but did not obtain a closed form solution. A closed form optimal solution for bearings-only multi-target localization was derived in [26]. Specifically, sensors were divided into multiple groups to localize diverse specific targets. However, each sensor can only acquire one target's signals only, and sensor sharing was not considered, which can acquire signals from multiple targets. Note that data association problem [27],[28],[29] may exist when the shared sensors obtain the measurements from different targets, and many methods can handle this situation [30],[31]. Furthermore, the work [32] studied the problem of shared sensors for two-target simultaneous, and found a geometrical solution of the optimal sensor placement.

It is worth mentioning that the above works have provided rigorous theoretical results about the optimal sensor placement, which can yield an elegant closed form solution in some cases. However, most sensor placement problems are nonconvex by nature. If some other constraints on the sensor locations are taken into consideration, then it is even harder to solve the formulated problems analytically as demonstrated in most of the existing works. Considering this, optimization-based and/or heuristic approaches have gained growing attention and been applied successfully recently. The average minimum detection time was proposed in [33] as the metric for water sensor placement, and the formulated problem was solved by the branch and bound method. In [34], two greedy algorithms were proposed to find the sensor locations, both of which select the locations one by one. Subsequently, [35] extended the greedy algorithms to a group-greedy strategy to further improve the solution performance at the expense of a larger search space. In [36], sensor selection was generalized to continuous sensor placement, which is relaxed into a convex problem and solved. In [37], a unified algebraic algorithm using the alternating direction method of multipliers (ADMM) was proposed for solving the optimal sensor placement for AOA, TOA, TDOA or RSS problems. The proposed frame can also be used for the optimization problem using different optimality criteria with realistic noise variances.

Apart from the solution methods, some challenges also arise due to the diversity of the localization scenarios in practice. Usually, for multiple target localization, the sensors are divided into several clusters, each of which is dedicated to a specific target. Besides, each sensor can only measure one target, and thus two classical methods were discussed and applied, viz., (i) using multiple sensors to localize different targets one-by-one; and (ii) using a larger number of sensors (with divided groups for different targets) to localize those targets simultaneously. In essence, the second method is still a localization method for a single target case, rather than for simultaneous multi-target localization. Both methods have limitations, such as low effectiveness and requiring a lot of sensors. Considering the cost or implementation limitations, a portion of the sensors serve as shared sensors to all these clusters, i.e., these shared sensors will participate in the localization of all targets. A concrete example for this scenario is a target localization sensor network that contains several static sensor stations as shared sensors and many mobile vehicles as non-shared sensors. This kind of sensor network is widely applied in undersea surveillance and indoor/outdoor area monitoring [38] [39] [40]. Consider, for example, a radar vehicle (regarded as a shared sensor) along with multiple unmanned aerial vehicles (UAVs) equipped with TOA sensors (regarded as non-shared sensors) to localize multi-targets in a large area. The radar vehicle is a command center for UAVs. However, this type of problem with practical meanings has not been well studied, and to the best of our knowledge, only the work [32] is available in the literature. In this paper, we extend the work in [32] to more general situations without the target number restriction. Furthermore, both the theoretical findings and a novel numerical optimization algorithm will be developed to formulate a hybrid approach. To clearly show the novelty of this paper, Table I comparing the characteristics of this work and other studies is provided.

TABLE I
COMPARISON BETWEEN SOME PREVIOUS STUDIES AND THIS PAPER.

Work	Target Number	Sensor Type
[6] N. H. Nguyen	Single	TOA, non-shared
[19] S. Xu	Single	TOA, non-shared
[25] D. Moreno-Salinas	Multiple	Range, non-shared
[26] Y. Li	Multiple	AOA, non-shared
[32] S. Xu	Two	TOA, mixed
This paper	Multiple	TOA, mixed

Work	Optimality Criterion	Solution Type
[6] N. H. Nguyen	D-Optimality	Analytical
[19] S. Xu	A-Optimality	Analytical
[25] D. Moreno-Salinas	D-Optimality	Analytical & numerical
[26] Y. Li	A-Optimality	Analytical
[32] S. Xu	A-Optimality	Analytical
This paper	A-Optimality	Analytical & numerical

The major contributions of this work can be summarized as follows:

- The optimal sensor placement problem for multi-target localization with shared sensors is studied for the first time to the best of our knowledge. The model and corresponding CRLB-based problem formulation are presented.

- For this formulated problem, a hybrid solution method is developed, which combines both the theoretical analysis and the numerical optimization. Based on the rigorous geometrical derivations, the analytical approaches can provide optimal and even closed form solutions for some special cases. When this approach is intractable, the proposed optimization-based numerical method can be the remedy in the sense that it can definitely provide a (sub-)optimal solution numerically. Thus, this hybrid solution approach can be deployed for most cases of sensor placement.
- Extensive simulations are conducted for various testing scenarios. The simulation results verify the correctness of the findings and proposed algorithms, which further demonstrates the efficacy of this proposed hybrid approach to sensor placement.

The rest of this paper is organized as follows. In Section II, the system model and the problem formulation are presented. Section III presents the analytical approach illustrated via theoretical results and special cases. An algorithm based on optimization techniques to the formulated problem is developed in Section IV. In Section V, a general optimal sensor placement solution is proposed. Subsequently, numerical simulations are conducted in Section VI, and the conclusions are drawn in Section VII.

Notation: Scalars, vectors and matrices are denoted by standard lowercase letter x, lower case boldface letter $\boldsymbol{x}$ and upper case boldface letter $\boldsymbol{X}$, respectively. $\mathbb{R}^n$ and $\mathbb{R}^{m\times n}$ denote the n-dimensional real-valued vector space and $m\times n$ real-valued matrix space, respectively. Subscripts $(\cdot)^T$ denotes the transpose operator. $\mathrm{Tr}\,(\cdot)$ and $\mathrm{vec}\,(\cdot)$ denote the trace and vectorization operators, respectively. $\boldsymbol{X}\succ\mathbf{0}$ ($\boldsymbol{X}\succeq\mathbf{0}$) represents that $\boldsymbol{X}$ is positive definite (positive semidefinite). $\mathrm{Diag}\,(\boldsymbol{x})$ stands for a diagonal matrix with its principal diagonal filled with $\boldsymbol{x}$. $\boldsymbol{I}_N$ denotes the $N\times N$ identity matrix. $\mathbf{1}_N$ denotes the $N\times 1$ vector with all elements being 1. x_i denotes the i-th element of $\boldsymbol{x}$. ∇ denotes the gradient.

II. Problem formulation

We consider the problem of optimal placement of TOA-based active sensors to localize K static targets simultaneously. The TOA measurements are taken from each sensor with a known location. We use $L=N_1+N_2...+N_K+M$ ($L\geq K+1$) sensors in total to localize K targets, where N_k sensors measure the kth target for $k=1,...,K$. M shared sensors can acquire the measurements from all K targets. Fig. 1 shows an example of the two-target localization problem with L sensors placed at locations with azimuth angles θ_{i1} where i is the sensor index. In order to make the problem tractable, we make three simplifying assumptions:

1) The TOA measurements are free from multipath and clutter.
2) Each measurement is correctly associated with the target, i.e., the data association problem is resolved.
3) The positions of the shared sensors are fixed, and the other sensors are installed on mobile vehicles.

In practical applications, TOA measurements might be affected by multipath and clutter interference, and many techniques have been developed to mitigate these effects. However, for the purpose of evaluating the fundamental performance, we have made assumption (1). Data association is always performed in multiple target localization. Similarly, a lot of solutions were explored in the literature. Thus, we make assumption (2) since these effects are handled by other methods, i.e., not in this paper. Assumption (3) provides a more general situation for target localization. Note that $N_1,N_2,...,N_K$ and M are manually determined. If $M=0$, i.e., no shared sensor exists, the localization problem will degenerate into multiple independent targets localization, and it can be resolved by the methods in [6] and [19].

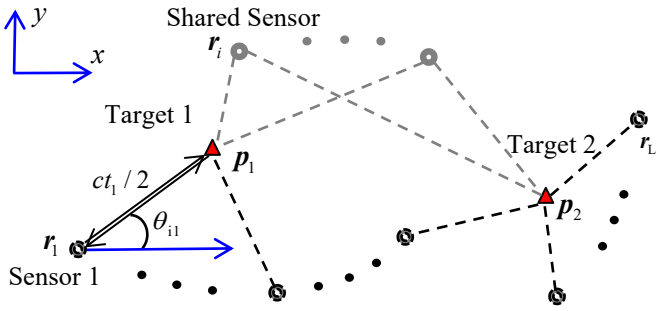


Fig. 1. Locating two targets simultaneously based on the TOA measurements.

The noisy TOA measurement $\tilde{t}_i$ of the ith sensor for target k takes the form

$$\tilde{t}_{ik}=t_{ik}+\eta_i=\frac{2\left\|\boldsymbol{p}_k-\boldsymbol{r}_i\right\|}{c}+\eta_{ik}, \tag{1}$$

where t_{ik} is the ideal measurement, c is the constant signal propagation speed and η_{ik} is assumed to be the additive independent Gaussian white noise (GWN) $\eta_{ik}\sim\mathcal{N}(0,\sigma_{ik}^2/c^2)$. $\boldsymbol{p}_k=[p_{xk},p_{yk}]^T$ denotes the target true position and $\boldsymbol{r}_i=[r_{xi},r_{yi}]^T$ is the ith sensor's position. Equation (1) can be written as

$$c\tilde{t}_{ik}=2\left\|\boldsymbol{p}_k-\boldsymbol{r}_i\right\|+c\eta_{ik} \tag{2}$$

and

$$\tilde{s}_{ik}=2d_{ik}+c\eta_{ik} \tag{3}$$

where $\tilde{s}_{ik}$ is the transformed noisy measurement, $d_{ik}=\|\boldsymbol{p}_k-\boldsymbol{r}_i\|$ denotes the target-sensor distance between the ith sensor and target k. The measurement noise satisfies $c\eta_{ik}\sim\mathcal{N}(0,\sigma_{ik}^2)$. At least two sensors for each target, i.e., $N_k+M=2$, are required to calculate the solution with prior knowledge.

Based on the above introduction, K sensor clusters exist for simultaneous localization of K targets, cluster k (or indicated as "group k") with N_k+M sensors will localize target k with the corresponding covariance matrix being $\boldsymbol{\Sigma}_k$. The covariance matrices can be diagonal or non-diagonal. For example, when the measurements of different sensors are uncorrelated (which is common), we have

$$\boldsymbol{\Sigma}_k=\mathrm{diag}\{\sigma_{1k}^2,\cdots,\sigma_{ik}^2,\quad\cdots,\sigma_{(N_k+M)k}^2\}_{(N_k+M)\times(N_k+M)} \tag{4}$$

for the kth target.

The Jacobian vector of the ith sensor measurement error evaluated at the true target k, i.e., $\boldsymbol{p}_k = [p_{xk}, p_{yk}]^T$, is

$$\begin{aligned}\boldsymbol{J}_{ik} &= \frac{\partial \tilde{s}_{ik}}{\partial \boldsymbol{p}^T}\Big|_{\boldsymbol{p}_1,\ldots,\boldsymbol{p}_K} \\ &= \left[\begin{array}{cccc} \frac{\partial \tilde{s}_{ik}}{\partial p_{x1}} & \frac{\partial \tilde{s}_{ik}}{\partial p_{y1}} & \cdots & \frac{\partial \tilde{s}_{ik}}{\partial p_{xk}} \\ \frac{\partial \tilde{s}_{ik}}{\partial p_{yk}} & \cdots & \frac{\partial \tilde{s}_{ik}}{\partial p_{xK}} & \frac{\partial \tilde{s}_{ik}}{\partial p_{yK}} \end{array}\right] \\ &= \left[\begin{array}{cccccccc} 0 & 0 & \cdots & 2\cos\theta_{ik} & 2\sin\theta_{ik} & \cdots & 0 & 0 \end{array}\right]\end{aligned} \tag{5}$$

where θ_{ik} is the azimuth angles between the true target k and the sensor as shown in Fig. 1. Note that if sensor i is a shared sensor, all the terms of $\boldsymbol{J}_{ik}$ will have the cos or sin functions (i.e., no zero terms). Since we assume the data association problem has already been solved (e.g., assuming the echo-signals from different targets have different frequencies), this shared sensor has multiple independent measurements (i.e., $\tilde{s}_{i1}, ..., \tilde{s}_{ik}, ...$ and $\tilde{s}_{iK}$). For locating K targets simultaneously, the Fisher information matrix $\boldsymbol{\Phi}$ [41] [42], is given by

$$\boldsymbol{\Phi} = \boldsymbol{J}_o^T \boldsymbol{\Sigma}_o^{-1} \boldsymbol{J}_o, \tag{6}$$

where

$$\begin{aligned}&\boldsymbol{J}_o = [\cdots, \boldsymbol{J}_{1k}^T, \cdots, \boldsymbol{J}_{(N_k+M)k}^T, \cdots]^T_{(N_1+\cdots+N_k+KM)\times 2K}, \\ &\boldsymbol{\Sigma}_0 = \left[\begin{array}{ccc} \boldsymbol{\Sigma}_1 & \cdots & \boldsymbol{0} \\ \vdots & \ddots & \vdots \\ \boldsymbol{0} & \cdots & \boldsymbol{\Sigma}_K \end{array}\right]_{(N_1+\cdots+N_k+KM)\times(N_1+\cdots+N_k+KM)},\end{aligned} \tag{7}$$

and the derivation is provided in Appendix A.

Assuming that the data association to the K targets is resolved, the performance of locating each target depends on the associate sensor cluster. We define

$$\boldsymbol{J}_k = \left[\boldsymbol{j}_{1k}, \ldots, \boldsymbol{j}_{N_k k}, \boldsymbol{j}_{(N_k+1)k}, \ldots, \boldsymbol{j}_{(N_k+M)k}\right]^T \tag{8}$$

with

$$\boldsymbol{j}_{ik} = \left[2\cos\theta_{ik}, 2\sin\theta_{ik}\right]^T. \tag{9}$$

Because the shared sensors are placed at fixed positions, their Jacobian vectors are fixed constants. The MSE is commonly used for unbiased estimation algorithms as an evaluation standard. We know that the A-optimality criterion, minimizing the trace of CRLB [tr(CRLB)], is equivalent to minimizing the MSE directly [19] [21] [43]. It is widely utilized and thus the A-optimality criterion is applied.

Then, the problem is formulated as

$$\underset{\{\boldsymbol{J}_k\}}{\text{minimize}} \quad \sum_{k=1}^{K} \text{Tr}\left[\left(\boldsymbol{J}_k^T \boldsymbol{\Sigma}_k^{-1} \boldsymbol{J}_k\right)^{-1}\right], \tag{10a}$$

$$\text{subject to} \quad \boldsymbol{j}_{ik}^T \boldsymbol{j}_{ik} = 4, \forall i \in \mathcal{I}_{own}^k \cup \mathcal{I}_{share}^k, \forall k \tag{10b}$$

$$\boldsymbol{j}_{tk} \text{ is fixed}, \forall t \in \mathcal{I}_{share}^k, \forall k, \tag{10c}$$

where $\mathcal{I}_{own}^k$ and $\mathcal{I}_{share}^k$ represent the set of N_k non-shared sensors and the set of M shared sensors for the k-th targets, respectively. Now, the objective is to find the geometrical solution (the values of θ_{ik}) of (10).

III. Simplification of (10) and Theoretical Solutions

The optimal sensor-target geometries will be found with given characteristics, i.e., d_{ik}, θ_{ik} and σ_{ik}^2. According to (6) and [24], the optimization problem in (10) equals

$$\begin{aligned}&\underset{\{\theta_{ik}\},\ i=1,\ldots,N_k,\ k=1,\ldots,K,\ t=1,\ldots,M}{\arg\min} \quad \text{tr}[(\boldsymbol{J}_o^T \boldsymbol{\Sigma}_o^{-1} \boldsymbol{J}_o)^{-1}], \\ &\text{s.t.} \quad \text{shared sensors locate at fixed positions, i.e., fixed } \theta_{tk}.\end{aligned} \tag{11}$$

We define

$$\boldsymbol{\Phi} = \boldsymbol{J}_o^T \boldsymbol{\Sigma}_o^{-1} \boldsymbol{J}_o = 4 \left[\begin{array}{ccccc} \mathcal{A}_1 & \mathcal{C}_1 & \ldots & \boldsymbol{0} & \boldsymbol{0} \\ \mathcal{C}_1 & \mathcal{B}_1 & \ldots & \boldsymbol{0} & \boldsymbol{0} \\ \vdots & \vdots & \ddots & \vdots & \vdots \\ \boldsymbol{0} & \boldsymbol{0} & \ldots & \mathcal{A}_K & \mathcal{C}_K \\ \boldsymbol{0} & \boldsymbol{0} & \ldots & \mathcal{C}_K & \mathcal{B}_K \end{array}\right]_{2K\times 2K}$$

$$\begin{aligned}\mathcal{A}_k &= \sum_{i=1}^{N_k} \frac{\cos^2\theta_{ik}}{\sigma_{ik}^2} + \sum_{t=1}^{M} \frac{\cos^2\theta_{tk}}{\sigma_{tk}^2}, \\ \mathcal{B}_k &= \sum_{i=1}^{N_k} \frac{\sin^2\theta_{ik}}{\sigma_{ik}^2} + \sum_{t=1}^{M} \frac{\sin^2\theta_{tk}}{\sigma_{tk}^2}, \\ \mathcal{C}_k &= \sum_{i=1}^{N_k} \frac{\cos\theta_{ik}\sin\theta_{ik}}{\sigma_{ik}^2} + \sum_{t=1}^{M} \frac{\cos\theta_{tk}\sin\theta_{tk}}{\sigma_{tk}^2}.\end{aligned} \tag{12}$$

Note that we use t to indicate the index of shared sensors specifically, i is to indicate the other sensors and k denotes the target index. Then, our objective is to find the solution of (11), and we get

Case 1: When $\boldsymbol{\Phi}$ is diagonal, the solution may be the global optimal.

Case 2: When $\boldsymbol{\Phi}$ is non-diagonal, the solution will be sub-optimal.

Consequently, we divide the optimization analysis into two cases.

A. Optimal Solution of Case 1

For case 1, the key problem is to make $\boldsymbol{\Phi}$ diagonal, i.e., $\mathcal{C}_k = \boldsymbol{0}$. Then, the global optimization problem becomes

$$\begin{aligned}&\underset{\{\theta_{ik} \text{ with fixed } \theta_{tk}\},\ i=1,\ldots,N_k,\ k=1,\ldots,K,\ t=1,\ldots,M}{\arg\min} \quad \text{tr}[(\boldsymbol{J}_o^T \boldsymbol{\Sigma}_o^{-1} \boldsymbol{J}_o)^{-1}] \\ &\text{s.t.} \quad \mathcal{C}_k = \boldsymbol{0}.\end{aligned} \tag{13}$$

In other words, the optimization has two steps. Firstly, we should make $\mathcal{C}_k = \boldsymbol{0}$, and secondly, we need to minimize the trace by adjusting the different sensor placements (θ_{ik}). Note that since the targets and shared sensors are fixed, θ_{tk} are fixed constants and we cannot change their values.

Therefore, the first task is to guarantee $\mathcal{C}_k = \boldsymbol{0}$ hold. In $\mathcal{C}_k$ of (12), the second term $\sum_{t=1}^{M} \frac{\cos\theta_{tk}\sin\theta_{tk}}{\sigma_{tk}^2}$ is a constant because the shared sensors are fixed. Consequently, the value of the first term should equals $-\sum_{t=1}^{M} \frac{\cos\theta_{tk}\sin\theta_{tk}}{\sigma_{tk}^2}$. Then, according to [44], we have $\frac{1}{a^2} + \frac{1}{b^2} \geq \frac{4}{a^2+b^2}$ with equality holding if $a^2 = b^2$. Then, combined with (12), the objective function in (11) becomes

$$\text{tr(CRLB)} \geq \sum_{k=1}^{K} \left(\frac{1}{4\mathcal{A}_k} + \frac{1}{4\mathcal{B}_k}\right) \geq \sum_{k=1}^{K} \frac{4}{4(\mathcal{A}_k + \mathcal{B}_k)} \tag{14a}$$

$$= \sum_{k=1}^{K} \frac{1}{\sum_{i=1}^{N_k} \frac{1}{\sigma_{ik}^2} + \sum_{t=1}^{M} \frac{1}{\sigma_{tk}^2}}, \tag{14b}$$

$$\text{s.t. } \mathcal{C}_k = \boldsymbol{0}, \tag{14c}$$

$$\mathcal{A}_k = \mathcal{B}_k. \tag{14d}$$

Next, we will find some special optimal placement strategies to reach the smallest tr(CRLB)= $\sum_{k=1}^{K} \frac{1}{\sum_{i=1}^{N_k} \frac{1}{\sigma_{ik}^2} + \sum_{t=1}^{M} \frac{1}{\sigma_{tk}^2}}$. Furthermore, it is interesting that an observation is found and concluded as below.

Observation: The smallest bound $\sum_{k=1}^{K} \frac{1}{\sum_{i=1}^{N_k} \frac{1}{\sigma_{ik}^2} + \sum_{t=1}^{M} \frac{1}{\sigma_{tk}^2}}$ is determined only by the measurement noise variances and sensor number, independent of the sensor placements, e.g., θ_{ik}, d_{ik}.

In other words, since the shared sensors are fixed, we need to guarantee the constraints (14c) and (14d) hold by placing the non-shared sensors in optimal positions. Once, the optimal sensor-target geometries are achieved, the optimal tr(CRLB) will be obtained automatically. We provide three special scenarios to derive some theoretical results.

Scenario 1: $M = 1$ and for the kth target, all the sensors have the same measurement noise variance σ_k^2.
For one target's echo signal, it is common to have a uniform measurement noise variance at multiple sensors (same quality). This special scenario may be the most common one compared with the others in practical applications. Based on the preliminary studies, some criteria of using N sensors in a single target localization problem will be applied (more details can be found in [6] [24] [32]).

Specifically, in the large SNR circumstance, we make the following remarks.

Remark 1. The optimal sensor placement criterion for single target localization is that $2\theta_i$ should have equal angular distribution or the distribution of $2\theta_i$ is symmetrical to the target.

Remark 2. The CRLB is invariant to rotation of all of the sensors simultaneously around the target, or flipping some sensors about the target for the 2D case.

Remark 3. The optimal CRLB of large SNR is independent of the sensor-target range for TOA localization.

Combined with these remarks, in this scenario, when $M = 1$, for each target, only one sensor's position is fixed while the other N_k sensors can be freely placed. Therefore, by appropriately adjusting the other sensors' positions, the optimal geometries can be always achieved. The detailed optimal placement strategy is included in Table II. Consequently, with the optimal geometries, the constraints in (14) are satisfied and the optimal bound becomes

$$\text{tr(CRLB)} = \sum_{k=1}^{K} \frac{\sigma_k^2}{N_k + M}. \tag{15}$$

TABLE II
DETERMINING THE OPTIMAL SENSOR PLACEMENT FOR SCENARIO 1.

Step 1: According to the position of the single shared sensor ($M = 1$), place N_k sensors around the kth target with the optimal sensor-target geometry based on Remark 1.
Step 2: Place $\sum_{k=1}^{K} N_k$ sensors for each target similarly.
Step 3: Adjust sensor positions based on Remarks 2 and 3 to avoid sensor collision problem. Then, the optimal geometries of the L sensors are determined and tr(CRLB)= $\sum_{k=1}^{K} \frac{\sigma_k^2}{N_k+M}$ is achieved.

Scenario 2: For the kth target, the number of non-shared sensors equals that of the shared sensors ($N_k = M$), and all the sensors have the same measurement noise variance σ_k^2.

In this scenario, the placements of the non-shared sensors should eliminate the impacts of the fixed shared sensors in the constraints of (14). Then, we divide the sensors into two groups, i.e., the fixed shared sensors and the non-shared sensors. Then, combined with the constraints in (12), we have

$$\sum_{i=1}^{N_k} \frac{\cos^2\theta_{ik}}{\sigma_k^2} + \sum_{t=1}^{M} \frac{\cos^2\theta_{tk}}{\sigma_k^2} = \sum_{i=1}^{N_k} \frac{\sin^2\theta_{ik}}{\sigma_k^2} + \sum_{t=1}^{M} \frac{\sin^2\theta_{tk}}{\sigma_k^2}, \tag{16a}$$

$$\sum_{i=1}^{N_k} \frac{\cos\theta_{ik}\sin\theta_{ik}}{\sigma_k^2} = -\sum_{t=1}^{M} \frac{\cos\theta_{tk}\sin\theta_{tk}}{\sigma_k^2}. \tag{16b}$$

By observing (16b), we find a solution of the optimal sensor placement as described in Table III. Also, combined with the **Observation**, the reachable optimal bound is

$$\text{tr(CRLB)} = \sum_{k=1}^{K} \frac{\sigma_k^2}{2M}. \tag{17}$$

TABLE III
DETERMINING THE OPTIMAL SENSOR PLACEMENT FOR SCENARIO 2.

Step 1: According to the determined positions of all the shared sensors, obtain $2\theta_{tk}$ for the kth target.
Step 2: Place the $N_k = M$ non-shared sensors to the positions that makes the distribution of $2\theta_{ik}$ and $2\theta_{tk}$ symmetrical to the target (similar to Remark 1).
Step 3: Adjust the non-shared sensors' positions based on Remarks 2 and 3 to avoid sensor collision problem.
Step 4: Place the non-shared sensors for the next target, until all the sensors are determined. Then, the optimal geometries of the L sensors are determined and tr(CRLB)= $\sum_{k=1}^{K} \frac{\sigma_k^2}{2M}$ is achieved.

Scenario 3: The angles of $M + N_k$ sensors, $2\theta_{jk}, j = 1, ..., M + N_k$, can have equal angular distribution or the distribution of $2\theta_{jk}$ is symmetrical to the target, and for the kth target, all the sensors have the same measurement noise variance σ_k^2.

In this scenario, the positions of the M shared sensors are very special and not easy to be satisfied. In other words, the fixed shared sensors must be firstly placed at special positions. Then, the other N_k sensors can be freely placed at their optimal positions. Thus, the constraints in (14) are satisfied and the optimal bound becomes tr(CRLB) = $\sum_{k=1}^{K} \frac{\sigma_k^2}{N_k+M}$. We provide an example for this scenario.

Suppose $K = 3$, $M = 3$, $N_1 = 2, N_2 = 1$, $N_3 = 1$ and $\sigma_{ik}^2 = \sigma_k^2$. An optimal sensor-target geometry is shown in Fig. 2, and an optimal sensor-target geometry is also shown. The optimal tr(CRLB) equals $\sum_{k=1}^{3} \frac{\sigma_k^2}{N_k+3}$. Besides, for $M = 2$ and $K = 2$ of scenario 3, the results are same to our previous work in [32].

In the simulation section, some detailed examples of the three scenarios will be provided.

B. Sub-optimal Solution of Case 2

If the FIM/CRLB cannot be diagonal, the optimization function degenerates to (10) or (11). Then, the only solution is to use the proposed optimization algorithm in Section IV.

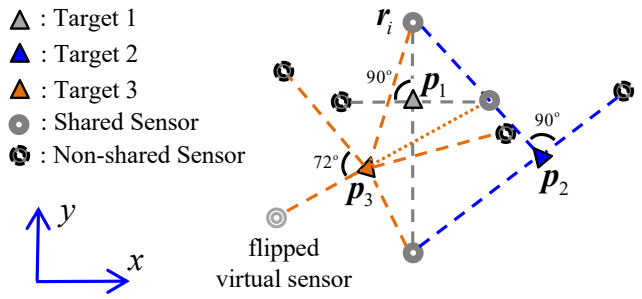


Fig. 2. An optimal geometry example of Scenario 3, where remarks 1, 2 and 3 are applied.

The global optimal placement is tough to achieve because of those strict constraints, e.g., (14). In addition, the theoretical bound tr(CRLB)= $\sum_{k=1}^{K}\frac{1}{\sum_{i=1}^{N_k}\frac{1}{\sigma_{ik}^2}+\sum_{t=1}^{M}\frac{1}{\sigma_{tk}^2}}$ may be hardly reached. Then, the proposed optimization algorithm in the next section can definitely find a sensor placement result and calculate a reachable lower bound. This is very important and meaningful for practical applications.

IV. Proposed Optimization Algorithm

A. Proposed Optimization Algorithm

The optimization problem in (10), it can be decomposed into K subproblems, each of which is given by

$$\begin{aligned}\underset{\boldsymbol{J}_k}{\text{minimize}} \quad & \operatorname{Tr}\left[\left(\boldsymbol{J}_k^T\boldsymbol{\Sigma}_k^{-1}\boldsymbol{J}_k\right)^{-1}\right]\\ \text{subject to} \quad & \boldsymbol{j}_{ik}^T\boldsymbol{j}_{ik}=4, \forall i\in\mathcal{I}_{own}^k\cup\mathcal{I}_{share}^k,\\ & \boldsymbol{j}_{tk} \text{ is fixed}, \forall t\in\mathcal{I}_{share}^k,\end{aligned} \tag{18}$$

The shared sensor is fixed and thus ignored in the derivation of the optimization algorithm. The following lemma presents an equivalent form of problem (18) in a maxi-min structure. By introducing an auxiliary variable $\boldsymbol{V}_k\in\mathbb{R}^{3\times 3}$, problem (18) is equivalent to

$$\begin{aligned}\underset{\boldsymbol{J}_k}{\text{maximize}} \quad & \min_{\boldsymbol{V}_k}\left\{\operatorname{Tr}\left(\boldsymbol{V}_k^T\boldsymbol{J}_k^T\boldsymbol{\Sigma}_k^{-1}\boldsymbol{J}_k\boldsymbol{V}_k\right)\right\}\\ \text{subject to} \quad & \operatorname{Tr}\left(\boldsymbol{V}_k\right)=1\\ & \boldsymbol{j}_{ik}^T\boldsymbol{j}_{ik}=4, \forall i\in\mathcal{I}_{own}^k.\end{aligned} \tag{19}$$

Proof. The inner minimization w.r.t. $\boldsymbol{V}_k$ of problem (19) is

$$\begin{aligned}\underset{\boldsymbol{V}}{\text{minimize}} \quad & \operatorname{Tr}\left(\boldsymbol{V}_k^T\boldsymbol{J}_k^T\boldsymbol{\Sigma}_k^{-1}\boldsymbol{J}_k\boldsymbol{V}_k\right)\\ \text{subject to} \quad & \operatorname{Tr}\left(\boldsymbol{V}_k\right)=1,\end{aligned} \tag{20}$$

which has the Lagrangian

$$\mathcal{L}\left(\boldsymbol{V}_k,\lambda\right)=\operatorname{Tr}\left(\boldsymbol{V}_k^T\boldsymbol{J}_k^T\boldsymbol{\Sigma}_k^{-1}\boldsymbol{J}_k\boldsymbol{V}_k\right)+\lambda\left(\operatorname{Tr}\left(\boldsymbol{V}_k\right)-1\right). \tag{21}$$

By using the Lagrangian method, we have

$$\begin{cases}\frac{\partial\mathcal{L}}{\partial\boldsymbol{V}}=2\boldsymbol{J}_k^T\boldsymbol{\Sigma}_k^{-1}\boldsymbol{J}_k\boldsymbol{V}_k+\lambda\boldsymbol{I}+\boldsymbol{G}=0\\ \frac{\partial\mathcal{L}}{\partial\lambda}=\operatorname{Tr}\left(\boldsymbol{V}_k\right)-1=0,\end{cases} \tag{22}$$

which has the solution

$$\begin{cases}\boldsymbol{V}_k^\star=\frac{\left(\boldsymbol{J}_k^T\boldsymbol{\Sigma}_k^{-1}\boldsymbol{J}_k\right)^{-1}}{\operatorname{Tr}\left[\left(\boldsymbol{J}_k^T\boldsymbol{\Sigma}_k^{-1}\boldsymbol{J}_k\right)^{-1}\right]}\\ \lambda^\star=\frac{-2}{\operatorname{Tr}\left[\left(\boldsymbol{J}_k^T\boldsymbol{\Sigma}_k^{-1}\boldsymbol{J}_k\right)^{-1}\right]}.\end{cases} \tag{23}$$

Substituting the expression of $\boldsymbol{V}_k^\star$ into the objective function of problem (20), we have

$$\operatorname{Tr}\left(\boldsymbol{V}_k^{\star T}\boldsymbol{J}_k^T\boldsymbol{\Sigma}_k^{-1}\boldsymbol{J}_k\boldsymbol{V}_k^\star\right)=\frac{1}{\operatorname{Tr}\left[\left(\boldsymbol{J}_k^T\boldsymbol{\Sigma}_k^{-1}\boldsymbol{J}_k\right)^{-1}\right]}. \tag{24}$$

Thus, problem (19) is equivalent to

$$\begin{aligned}\underset{\boldsymbol{J}}{\text{maximize}} \quad & \frac{1}{\operatorname{Tr}\left[\left(\boldsymbol{J}_k^T\boldsymbol{\Sigma}_k^{-1}\boldsymbol{J}_k\right)^{-1}\right]}\\ \text{subject to} \quad & \boldsymbol{j}_{ik}^T\boldsymbol{j}_{ik}=4, \forall i\in\mathcal{I}_{own}^k.\end{aligned} \tag{25}$$

which is further equivalent to problem (18), thereby completing the proof. □

Hereafter, we focus on solving problem (19), for which we resort to the alternating gradient projection approach. For a fixed $\boldsymbol{J}_k^\ell$ at the ℓ-th iteration, the minimization problem w.r.t. $\boldsymbol{V}_k$ is

$$\begin{aligned}\underset{\boldsymbol{V}_k}{\text{minimize}} \quad & \operatorname{Tr}\left[\boldsymbol{V}_k^T\left(\boldsymbol{J}_k^\ell\right)^T\boldsymbol{\Sigma}_k^{-1}\boldsymbol{J}_k^\ell\boldsymbol{V}_k\right]\\ \text{subject to} \quad & \operatorname{Tr}\left(\boldsymbol{V}_k\right)=1,\end{aligned} \tag{26}$$

which has a closed form solution given by

$$\boldsymbol{V}_k^{\ell+1}=\frac{\left[\left(\boldsymbol{J}_k^\ell\right)^T\boldsymbol{\Sigma}_k^{-1}\boldsymbol{J}_k^\ell\right]^{-1}}{\operatorname{Tr}\left[\left(\left(\boldsymbol{J}_k^\ell\right)^T\boldsymbol{\Sigma}_k^{-1}\boldsymbol{J}_k^\ell\right)^{-1}\right]}. \tag{27}$$

For the fixed $\boldsymbol{V}^{\ell+1}$, the maximization problem w.r.t. $\boldsymbol{J}$ is

$$\begin{aligned}\underset{\boldsymbol{J}}{\text{maximize}} \quad & \operatorname{Tr}\left[\left(\boldsymbol{V}_k^{\ell+1}\right)^T\boldsymbol{J}_k^T\boldsymbol{\Sigma}_k^{-1}\boldsymbol{J}_k\boldsymbol{V}_k^{\ell+1}\right]\\ \text{subject to} \quad & \boldsymbol{j}_{ik}^T\boldsymbol{j}_{ik}=4, \forall i\in\mathcal{I}_{own}^k,\end{aligned} \tag{28}$$

which has the projection update rule given by

$$\begin{aligned}\boldsymbol{j}_{ik}^{\ell+1}=&2\mathcal{P}_{\mathcal{J}}\left(\boldsymbol{j}_{ik}^\ell+\alpha\left(\boldsymbol{V}_k^{\ell+1}\left(\boldsymbol{V}_k^{\ell+1}\right)^T\left(\boldsymbol{J}_k^\ell\right)^T\boldsymbol{\Sigma}_k^{-1}\right)_{i,:}\right),\\ &\forall i\in\mathcal{I}_{own}^k,\end{aligned} \tag{29}$$

where $(\cdot)_{i,:}$ represents the i-th column of a matrix, $\mathcal{P}_{\mathcal{J}}(\cdot)$ represents the normalization operation and $\alpha>0$ is the stepsize.

We solve problem (18) by updating $\boldsymbol{V}_k$ and $\boldsymbol{J}_k$ via (27) and (29) until convergence. Recall that the original problem (10) can be decomposed into K subproblems like (18). The summary of the complete algorithm to problem (10) is given in Algorithm IV, where the objective value of problem (18) is denoted by f_k.

B. Convergence of the Proposed Algorithm

We analyze the convergence of the proposed algorithm to solve the optimization problem in (18). For notational simplicity, we ignore the subscript k and some fixed constraints. For each target, we have the following problem:

$$\begin{aligned}\underset{\boldsymbol{J}}{\text{minimize}} \quad & \operatorname{Tr}\left[\left(\boldsymbol{J}^T\boldsymbol{\Sigma}^{-1}\boldsymbol{J}\right)^{-1}\right]\\ \text{subject to} \quad & \boldsymbol{j}_i^T\boldsymbol{j}_i=4, \forall i=1,\ldots N.\end{aligned} \tag{30}$$

TABLE IV
PROPOSED ALGORITHM FOR OPTIMAL SENSOR PLACEMENT WITH SHARED SENSORS

Input: Covariance matrices $\{\boldsymbol{\Sigma_k}\}_{k=1}^K$, initial $\{\boldsymbol{J}_k^0\}_{k=1}^K$, convergence threshold ε, stepsize α,
Output: Convergened sensor location vector $\boldsymbol{j}_{ik}, \forall i \in \mathcal{I}_{own}^k$ with $k = 1, \ldots, K$,

1: **for** $k = 1, \ldots, K$ in parallel **do**
2: **repeat**
3: update $\boldsymbol{V}_k^{\ell+1}$ via (27)
4: update $\boldsymbol{j}_{ik}^{\ell+1}$ via (29)
5: $\ell \leftarrow \ell + 1$
6: **until** $\left(\left|f_k^{\ell+1} - f_k^{\ell}\right|\right) / \left|f_k^{\ell}\right| \leq \varepsilon$
7: **end for**

First, we have the following lemma.

Lemma 1. When $\boldsymbol{\Sigma}$ is diagonal, solving problem (30) is equivalent to solving

$$\begin{aligned} \underset{\boldsymbol{J}}{\text{maximize}} \quad & \min_{\text{Tr}(\boldsymbol{V})=1, \boldsymbol{V} \succeq \boldsymbol{0}} \left\{\text{Tr}\left(\boldsymbol{V}^T \boldsymbol{J}^T \boldsymbol{\Sigma}^{-1} \boldsymbol{J} \boldsymbol{V}\right)\right\} \\ \text{subject to} \quad & \boldsymbol{j}_i^T \boldsymbol{j}_i \leq 4, \forall i = 1, \ldots, N. \end{aligned} \tag{31}$$

Proof: Since $\boldsymbol{\Sigma}$ is diagonal, $\boldsymbol{\Sigma} = \text{Diag}\left(\boldsymbol{r} \odot \boldsymbol{r}\right)$ with an unique $\boldsymbol{r} > \boldsymbol{0}$, where $\odot$ represents the Hadamard product. Then problem (31) can be rewritten as, by setting $\hat{\boldsymbol{J}} = \text{diag}\left(\boldsymbol{r}\right) \boldsymbol{J}$,

$$\begin{aligned} \underset{\boldsymbol{J}}{\text{maximize}} \quad & \min_{\text{Tr}(\boldsymbol{V})=1, \boldsymbol{V} \succeq \boldsymbol{0}} \left\{\text{Tr}\left(\boldsymbol{V}^T \hat{\boldsymbol{J}}^T \hat{\boldsymbol{J}} \boldsymbol{V}\right)\right\} \\ \text{subject to} \quad & \hat{\boldsymbol{j}}_i^T \hat{\boldsymbol{j}}_i \leq 4 r_i^2, \forall i = 1, \ldots, N. \end{aligned} \tag{32}$$

Assume that the optimal solution to problem (32) is $\left(\hat{\boldsymbol{J}}^\star, \boldsymbol{V}^\star\right)$ with $\left\|\hat{\boldsymbol{j}}_i^\star\right\|^2 < 4r_i^2, \forall i$. The objective value of the maximization problem is

$$\text{Tr}\left(\boldsymbol{V}^{\star T} \hat{\boldsymbol{J}}^{\star T} \hat{\boldsymbol{J}}^\star \boldsymbol{V}^\star\right) = \text{Tr}\left(\hat{\boldsymbol{J}}^\star \boldsymbol{V}^\star \boldsymbol{V}^{\star T} \hat{\boldsymbol{J}}^{\star T}\right) = \sum_{i=1}^N \hat{\boldsymbol{j}}_i^{\star T} \hat{\boldsymbol{j}}_i^\star. \tag{33}$$

For each term $\hat{\boldsymbol{j}}_i^{\star T} \boldsymbol{V}^\star \boldsymbol{V}^{\star T} \hat{\boldsymbol{j}}_i^\star$, the value of the term can be further increased by scaling $\hat{\boldsymbol{j}}_i^\star$ to meet $\hat{\boldsymbol{j}}_i^T \hat{\boldsymbol{j}}_i = 4r_i^2$, which conflicts the assumption that $\left(\hat{\boldsymbol{J}}^\star, \boldsymbol{V}^\star\right)$ is optimal with $\left\|\hat{\boldsymbol{j}}_i^\star\right\|^2 < 4r_i^2, \forall i$. Thus, solving problem (31) is equivalent to solving

$$\begin{aligned} \underset{\boldsymbol{J}}{\text{maximize}} \quad & \min_{\text{Tr}(\boldsymbol{V})=1, \boldsymbol{V} \succeq \boldsymbol{0}} \left\{\text{Tr}\left(\boldsymbol{V}^T \boldsymbol{J}^T \boldsymbol{\Sigma}^{-1} \boldsymbol{J} \boldsymbol{V}\right)\right\} \\ \text{subject to} \quad & \boldsymbol{j}_i^T \boldsymbol{j}_i = 4, \forall i = 1, \ldots N, \end{aligned} \tag{34}$$

which is further equivalent to problem (30) according to Lemma 1. Therefore, the proof is completed. ■

Now, the convergence of the proposed algorithm can be derived by analyzing (31), which is given in the following theorem.

Theorem 1. Let $\left\{\boldsymbol{J}^\ell\right\}$ be the sequence generated by the proposed algorithm. Then every limit point of the sequence $\left\{\boldsymbol{J}^\ell\right\}$ is a stationary point of problem (30).

Proof: Let $g\left(\boldsymbol{J}\right) = \min_{\boldsymbol{V} \in \mathcal{V}} \left\{\text{Tr}\left(\boldsymbol{V}^T \boldsymbol{J}^T \boldsymbol{\Sigma}^{-1} \boldsymbol{J} \boldsymbol{V}\right)\right\}$, $f\left(\boldsymbol{J}, \boldsymbol{V}\right) = \text{Tr}\left(\boldsymbol{V}^T \boldsymbol{J}^T \boldsymbol{\Sigma}^{-1} \boldsymbol{J} \boldsymbol{V}\right)$. The function $f\left(\boldsymbol{J}, \boldsymbol{V}\right)$ is differentiable in $\boldsymbol{J}$ for $\boldsymbol{j}_i^T \boldsymbol{j}_i \leq 4$. Furthermore, $f\left(\boldsymbol{J}, \boldsymbol{V}\right)$ is strongly convex in $\boldsymbol{V}$ and the set $\mathcal{V} = \left\{\boldsymbol{V} | \text{Tr}\left(\boldsymbol{V}\right) = 1, \boldsymbol{V} \succeq \boldsymbol{0}\right\}$ is compact. Thus, problem (31) satisfies the assumptions of Danskin's Theorem [45], by which we have $\nabla g\left(\boldsymbol{J}\right) = \nabla f\left(\boldsymbol{J}, \boldsymbol{V}^\star\right)$ with $\boldsymbol{V}^\star = \arg \min_{\text{Tr}(\boldsymbol{V}) \leq 1} \left\{\text{Tr}\left(\boldsymbol{V}^T \boldsymbol{J}^T \boldsymbol{\Sigma}^{-1} \boldsymbol{J} \boldsymbol{V}\right)\right\}$.

Then, the update rule of the proposed algorithm is reduced to $\boldsymbol{J}^{\ell+1} = \mathcal{P}_{\mathcal{J}}\left(\boldsymbol{J}^\ell - \alpha \nabla g\left(\boldsymbol{J}\right)\right)$. By applying the Theorem in [46] with $\epsilon = 0$ (due to the availability of the optimal $\boldsymbol{V}$), we arrive at the conclusion that the sequence $\left\{\boldsymbol{J}^\ell\right\}$ will converge to the stationary point of $g\left(\boldsymbol{J}\right)$, which has $\nabla g\left(\boldsymbol{J}\right) = 0$. ■

Thus, the proposed method will always converge to the (sub-)optimal results for each target. Further, the sensor placements will converge to a (sub-)optimal sensor-target geometry.

V. THEORETICAL AND MATHEMATICAL HYBRID METHOD

A. The Hybrid Method

By integrating the proposed method in Sections III and IV, in this section, we develop a general hybrid strategy to quickly determine the optimal placement.

The theoretical method in Section III can simply offer the solutions for the special scenarios. For the more general cases, the numerical algorithm proposed in Section IV can always provide (sub-)optimal solutions. Besides, the theoretical method can be applied to quickly determine an initial placement of the different non-fixed sensors which will provide a good initial point for the numerical algorithm for the sake of convergence speed. More specifically, some assumptions can be made to simplify the cases that do not satisfy the special scenarios, and quickly obtain an optimal placement of the approximated cases. Then, this placement can be applied as the initial guess of the proposed optimization algorithm. To summarize, the details of the general solution of the hybrid method are introduced in Fig. 3.

B. Extension to Mobile Target Scenarios

The proposed method can be extended to dynamic target scenarios by capturing the real-time sensor-target geometries and evaluating the estimation performance for optimal mobile sensor placement at each time instant. A proposed extended method has four steps and the pseudo codes are shown in Table V.

TABLE V
EXTENDED METHOD FOR MOVING TARGET PROBLEM BASED ON THE PROPOSED METHOD.

Step 1: Optimize the sensor placement based on the initial estimated target positions using initial measurements. Give initial guesses of targets' velocities (e.g., all zeros).
Step 2: When targets move during one sampling time interval, update the targets' position estimates based on the previous estimated positions and velocities.
Step 3: Re-calculate the optimal sensor placement using the proposed method in Fig. 3. Change the real-time sensor-target geometries by moving the non-shared sensors and obtain new measurements.
Step 4: Update the real-time estimated multi-target positions and velocities using the new measurements. Go back to Step 2 for the next time instant.

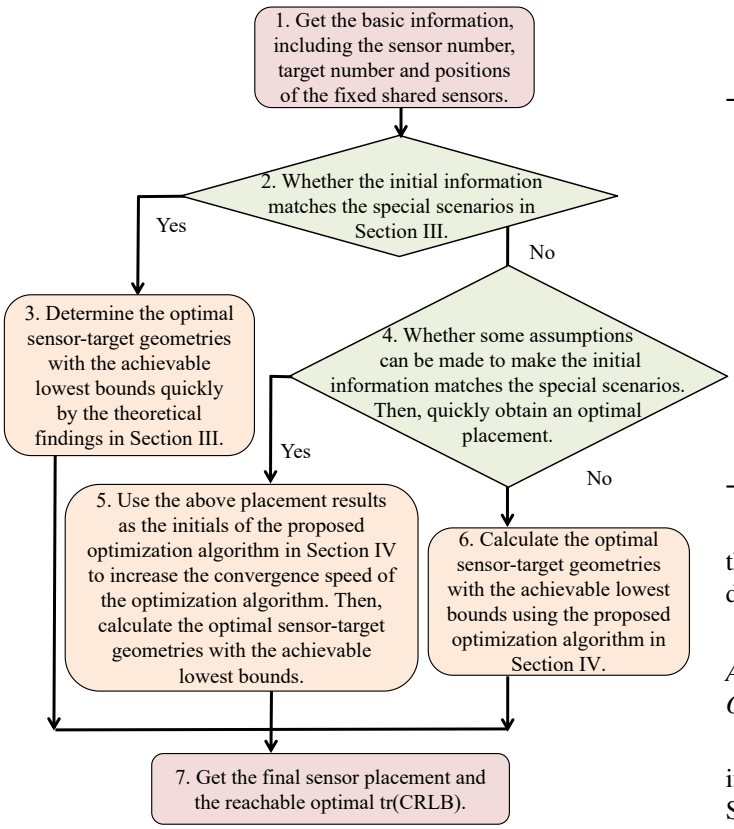


Fig. 3. The diagram of the hybrid method.

Furthermore, for mobile target tracking, the posterior CRLB (PCRLB) will be the most appropriate benchmark, which is also provided in Appendix C. We can see clearly that the PCRLB is also related to the sensor-target geometry, and thereby, the sensor placement also makes sense. Considering the space and scope of this paper, it will be explored in future work.

C. Extension to Data Association Scenarios

In this subsection, we will extend the proposed sensor placement method to a case with data association. Apart from using the classical algorithms [27],[28],[29], we propose a method to overcome the data association by using the measurements acquired from the mobile non-shared sensors. In other words, the key idea is to use the measurements of the mobile non-shared sensors to resolve the data association that existed only in the shared sensors. This results in a five-step pseudo-code for data association which is summarized in Table VI.

TABLE VI
EXTENDED SOLUTION OF DATA ASSOCIATION PROBLEM USING THE PROPOSED METHOD.

Step 1: Randomly place and move the non-shared sensors, and get diverse measurements to calculate a rough position of a target.
Step 2: Repeat Step 1 for all clusters until acquire all targets' rough positions.
Step 3: Compare the estimated target positions and each shared sensors' multiple measurements, a preliminary relation between the measurements and target indices is obtained.
Step 4: Optimize the sensor placement using the proposed method (Fig. 3). Get new measurements from all the sensors to calculate the targets positions with improved accuracy.
Step 5: Repeat Steps 3 and 4 multi-times, double-check the measurement-target relationship.

VI. SIMULATION STUDIES

In this section, we verify the correctness of the proposed theoretical optimal placement method, the effectiveness of the developed optimization algorithm and the hybrid method. Then, some practical target localization problems using different estimation algorithms are provided to demonstrate the superiority of the optimal sensor-target geometries. Consequently, the findings and the proposed algorithms are verified, and the utility of the proposed methods in practical applications is demonstrated.

A. Demonstrations of the Theoretical Findings and Proposed Optimization Algorithm

In this subsection, we provide some examples of the different scenarios. The proposed optimization algorithm in Section IV is applied to each example. The trajectories of the mobile non-shared sensors and tr(CRLB)s are both recorded. Then, we compare the final sensor-target geometries & tr(CRLB)s and the derived theoretical results in Sections III. Since the distance does not impact the final tr(CRLB), the sensor-target distances are constants.

For Scenario 1, we assume $M = 1$, $N_1 = 1, N_2 = 1$ and $N_3 = 2$ (total 5 sensors) to localize $K = 3$ targets, and the measurement noise standard deviations are $\sigma_1 = 1$m, $\sigma_2 = 1.5$m and $\sigma_3 = 2.5$m. The true targets' positions are $(0, 0)$m, $(300, 0)$m and $(300, 300)$m. Then, an example is provided. In example 1, the shared sensor is placed randomly at a fixed position. Since the distance does not impact the final tr(CRLB), the non-shared sensors of each target are constrained to be placed at the same distance between the shared sensor and each target. The non-shared sensors start from some randomly selected positions, and the proposed optimization algorithm in Section IV is applied. Consequently, the convergence process of all the mobile sensors' trajectories are acquired and shown in Fig. 4(a). The objective function of example 1, i.e., tr(CRLB), finally converges to 3.7084m^2. According to (15), the theoretical optimal tr(CRLB)= 3.7083m^2. Besides, the final geometry in Fig. 4(a) matches the findings in Table II.

For Scenario 2, $K = 3$ targets are to be localized, and $N_1 = N_2 = N_3 = M = 2$, i.e., a total of 8 sensors are used. The measurement noise standard deviations are $\sigma_1 = 1$m, $\sigma_2 = 1.5$m and $\sigma_3 = 2.5$m. The true targets' positions are $(0, 0)$m, $(300, 0)$m and $(300, 300)$m. The distance between the shared sensors and target 1 is 100m, and then we randomly place the 2 shared fixed sensors around target 1. The sensor-target radii of the other sensors and the other 2 targets, equal the distances between the target and one randomly selected

fixed shared sensor. We randomly place the 2 shared sensors as in example 2. Similar to example 1, the proposed optimization algorithm is applied. The final sensor-target geometry is shown in Fig. 4(b), and the actual tr(CRLB)s of example 3 equals 2.3751m^2. The theoretical lower bound is tr(CRLB)$=$ 2.3750 m^2 based on (16b). Furthermore, the optimal sensor placement demonstrates the effectiveness of the proposed placement method in Table III.

For Scenario 3, we simulate example 3 illustrated in Fig. 2 with $K = 3$, $M = 3$, $N_1 = 2, N_2 = 1$ and $N_3 = 1$, $\sigma_1 = 1$m, $\sigma_2 = 1.5$m and $\sigma_3 = 2.5$m. More specifically, the locations of the three targets are $(-63.62, -130.47)$, $(0, 0)$ and $(200, -100)$m. The positions of the fixed shared sensors are $(0, 100)$, $(0, 100)$ and $(0, -400)$m. Applying the proposed optimization algorithm produces the final sensor-target geometry shown Fig. 4(c). The actual tr(CRLB) of example 3 equals 2.0625m^2 which is the same as the theoretical smallest tr(CRLB)$=$ 2.0625m^2.

TABLE VII
THE THEORETICAL TR(CRLB)S AND CALCULATED TR(CRLB)S OF THE 3 EXAMPLES.

Example	Theoretical tr(CRLB)	Optimized tr(CRLB)
1	3.7083m^2	3.7084m^2
2	2.3750m^2	2.3751m^2
3	2.0625m^2	2.0625m^2

The theoretical tr(CRLB) and the results of the proposed optimization algorithm for the three scenarios considered are listed in Table VII. The optimal sensor-target geometry solutions are obtained using steps 1, 2, 3 and 7 in Fig. 3. It is clear that the optimization algorithm can always obtain the geometries with the optimal bounds in the three scenarios. In summary, the effectiveness of the proposed optimization algorithm in Section IV is verified. In addition, the correctness of the proposed methods for finding the optimal sensor-target geometries in Tables II and III is confirmed.

B. Verification of the Hybrid Method

To verify the proposed hybrid method in Section V, a special situation which, is introduced in Section III.B and does not match the previous three scenarios, is provided as scenario 4. In this case the theoretical results of Section III.A cannot be applied directly. However, an approximate optimal solution, based on the theoretical results, can be used to initialize the optimization algorithm in Section IV. The solution follows steps 1, 2, 4, 5 and 6 in Fig. 3.

In Scenario 4, we assume $K = 3$ targets, and $N_1 = N_2 = N_3 = M = 2$, i.e., a total of 8 sensors. The measurement noise standard deviations σ_{ik} of the sensors are different. This represents a more general situation because sensors have different characteristics. We assume sensors 1 and 2 are the fixed shared sensors. Sensors 3 and 4 are clustered to locate target 1, sensors 5 and 6 target 2, and sensors 7 and 8 target 3. The sensor noise standard deviations are $\sigma_{11} = 1$m, $\sigma_{21} = 1.2$m, $\sigma_{31} = \sigma_{41} = 1.5$m, $\sigma_{12} = 2$m, $\sigma_{22} = 1.5$m, $\sigma_{52} = 2.5$m, $\sigma_{62} = 2.8$m, $\sigma_{13} = \sigma_{23} = \sigma_{73} = 2.5$m and $\sigma_{83} = 3$m. The true target positions are $(0, 0)$m, $(300, 0)$m and $(300, 300)$m. The other conditions are the same as those in example 2.

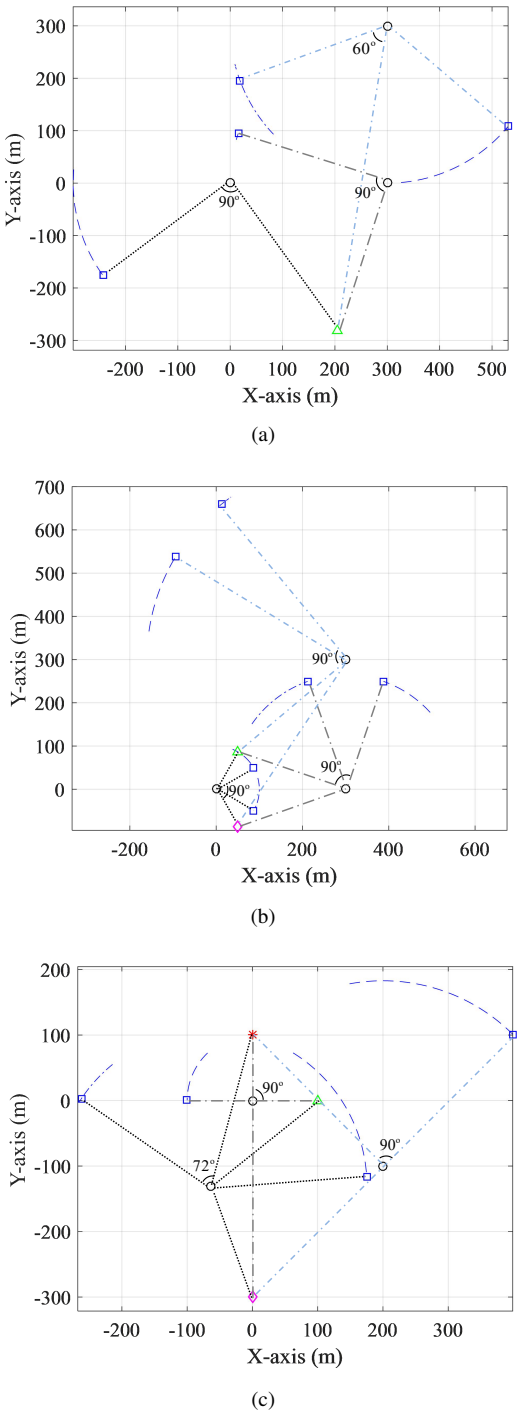


Fig. 4. The optimal geometries calculated using the proposed algorithms, (a) example 1, (b) example 2 and (c) example 3. One black ○ denotes a target. The green △, pink ◇ and red ∗ denote the fixed shared sensors. One blue □ denotes the final position of a non-shared sensor. The blue dash lines are the sensors' trajectories in the optimal placement calculation algorithms.

Using the hybrid method, we first assume for each target

the sensor measurement variance is uniform, i.e, the special case of scenario 2 holds. Thus, we can quickly obtain the approximate optimal placement based on Table III, which gives the same result as in example 2. Consequently, we substitute this placement as an initialization for the proposed numerical optimization algorithm and calculate the final optimal solution. The result acquired by this optimization process is labeled case 1. For comparison purposes, the result of the optimization algorithm using randomly selected initial placement is referred to as case 2. Similarly, the result of the optimization algorithm using nearly uniform initial placement is labeled case 3. Fig. 5 shows the optimization results for the three cases. It is interesting to note that the three optimal geometries in Fig. 5 only differ by the flipping of some non-shared sensors about targets, which does not change the optimality of sensor-target geometries (see Remark 2). In other words, the proposed optimization algorithm matches the theoretical findings properly.

The convergence speeds and final bounds of these 3 cases are provided and compared in Table VIII. We applied a threshold ($\varepsilon = 10^{-5}$ introduced in Table IV), and thus when the objective function's values of two consecutive iterations satisfy the stop threshold, the convergence process completes. Note that we use the total convergence iteration number in the proposed algorithm as an evaluation of the convergence speed. The hybrid method uses the least number of iterations to converge to the lowest bound. The proposed optimization algorithm converges to the theoretical tr(CRLB), which verifies the effectiveness of our method. In addition, the proposed method can be applied for the cases with a large number of sensors or targets.

TABLE VIII
THE CONVERGENCE SPEED AND FINAL TR(CRLB) OF THE 3 CASES IN EXAMPLE 4.

Case	Convergence iteration number	Optimized tr(CRLB)
1	799	3.1877m^2
2	1078	3.1877m^2
3	1022	3.1877m^2

Furthermore, according to Fig. 3, the proposed algorithm can calculate the final (sub-)optimal placement, if neither the theoretical results nor the approximated initialization can be applied. Specifically, the solution follows steps 1, 2, 4, 6 and 7. This is verified by cases 2 and 3 simulated above (shown in Fig.5).

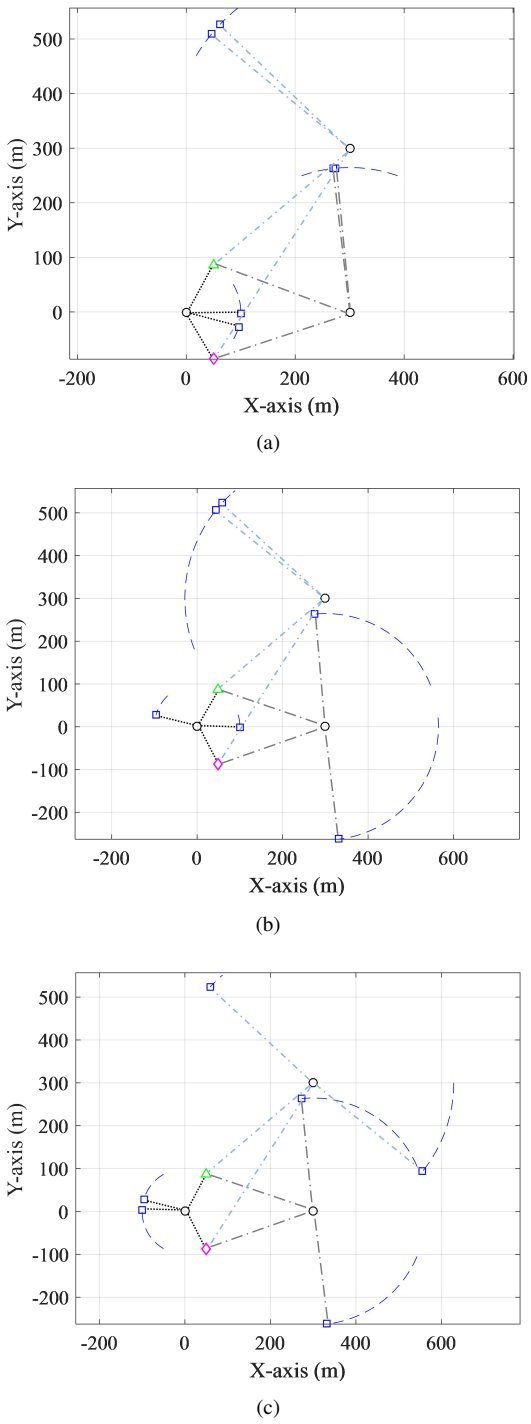


Fig. 5. The optimal geometries calculated using the hybrid method of example 4. (a) case 1 using approximated optimal placement initial, (b) case 2 using random placement initial, (c) case 3 using nearly uniform placement initial. One blue □ denotes the final position of a non-shared sensor. The blue dash lines are the sensors' trajectories in the optimal placement calculation algorithms.

C. Practical Comparisons between Optimal and Non-optimal Sensor-target Geometries

To verify the findings in some practical applications, we estimate multiple target locations in the previous three scenarios using the extended Kalman filter (EKF) and maximum likelihood estimator (MLE). The EKF and MLE are two commonly used unbiased iterative and non-iterative estimators, respectively. Even in the cases of non-uniform sensors, the diverse variances σ_{ik}^2 are clearly known, and thus some modifications are made in the estimators. In the MLE, the probability density function (PDF) also considers the known diverse variances. In the examples, the optimal sensor-target geometries are first determined by the proposed scheme in Tables II and III as depicted in Figs. 4(a)-4(c). Then, a few

non-optimal geometries are selected for comparison. The tru target locations are the same as those in the three examples More specifically, the non-optimal geometries are acquire by making some sensors deviate from their optimal position (refer to [32] and [19]).

The initial estimates of the three target locations are dif ferent from the true states and the covariance matrices ar all $\mathrm{diag}[10, 0, 10, 0]$. The measurement noise variances ar $\sigma_{i1}^2 = 1^2$ m^2, $\sigma_{i2}^2 = 1.5^2$ m^2 and $\sigma_{i3}^2 = 2.5^2$ m^2. In the EKI 50 successive TOA measurements for each target are use to estimate the targets. The mean-squared-error calculated b the true target and estimated states [47] is used to evaluat the estimation performance. In each example, the estimatio process is repeated using 1000 Monte Carlo runs and th performance is averaged over the Monte Carlo data. "OP" an "Non-OP" denote the optimal and non-optimal geometrie A green $\triangle$ denote a fixed shared sensor, a red $*$ means target and a blue $\diamond$ denotes a non-shared sensor. The detaile geometries and final estimation performance of the differer geometries are shown in Figs. 6-8. Note that the EKF may not converge to the theoretical tr(CRLB). However, these figures still imply that the "OP" geometries can provide optimal performance. Furthermore, for the iterative estimator, the corresponding posterior CRLB (PCRLB) matrix is also derived in Appendix C. The trace values of the PCRLB of examples 1-3 with 1000 Monte Carlo runs are shown in Figs. 6-8 as well. Note that for different sensor-target geometries, diverse PCRLB matrices exist, and we only draw the tr(PCRLB) of the optimal geometry.

Next, we use a maximum likelihood estimator (MLE) to estimate the target locations, which is a batch estimator and its estimation variance can asymptotically achieve the theoretical tr(CRLB). A grid-search method and a single-iteration Gauss-Newton (GN) algorithm [48] are utilized in the MLE. We calculate the mean-squared-error (MSE) from the target estimates and true values using 10,000 Monte Carlo simulations. For the sensor-target geometries in Figs 6-8, the performance of the MLE is shown in Figs. 9-11. The MSEs for the optimal geometries (OP) get very close to the theoretical tr(CRLB), which confirms the lower bounds derived in Sections III and IV.

According to the derivations in this paper, the optimal tr(CRLB) in (10) is a function of the sensor-target geometries, i.e., θ_{ik}. Thus, there is a nonlinear relationship between the sensor placement and the optimal tr(CRLB). With appropriate sensor and target numbers, the lower bound's sensitivity of the sensor placement may be robust, such that the achievable bound will not increase too much when small perturbation in sensor locations happens. Based on the simulation results, especially in Figs. 9-11, a simple observation is made, that the robustness of the optimal sensor locations will be improved as the ratio of sensor-target numbers ($\frac{\text{sensor number}}{\text{target number}}$) increases. A rigorous theoretical study may be a challenging topic as an extension in the future.

D. Simulation Examples of Extended Cases

In this subsection, two examples are provided to verify the effectiveness of the proposed method in Section V.B and V.C,

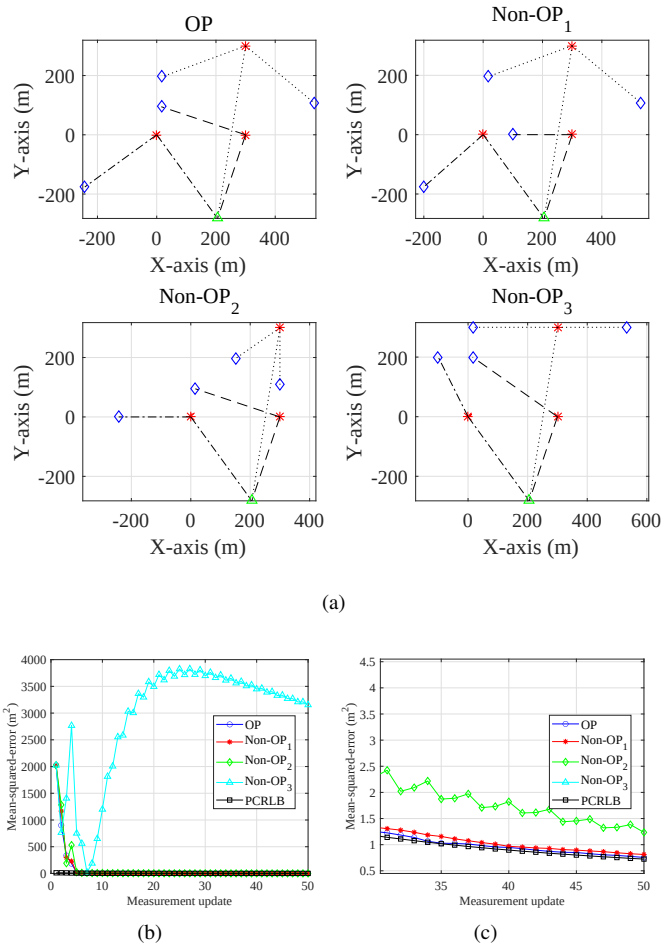
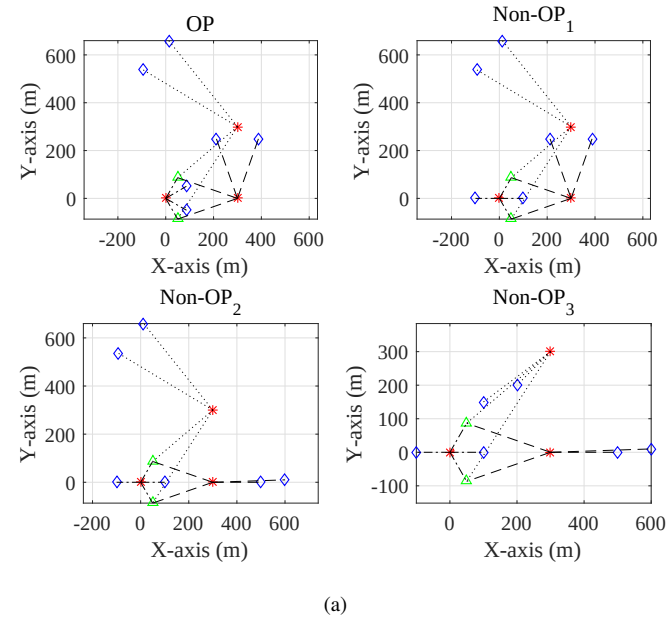


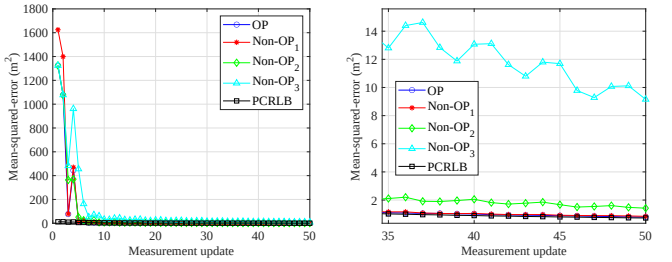
Fig. 6. EKF results of example 1, (a) different geometries, (b) performance (c) zoom view.

i.e., the cases of tracking mobile targets and considering data association.

For example 5, two mobile targets will be estimated using the classical EKF algorithm. The two targets move from $(0, 0)$m and $(300, 0)$m with velocities $(5, 0)$m/s and $(3, -3)$m/s, respectively. We assume $M = 1$, $N_1 = 1$ and $N_2 = 1$ (total 3 sensors) to localize $K = 2$ targets, and the measurement noise standard deviations of different sensors are uniform with $\sigma = 1.5$m. The EKF initial states are given with some deviations from the true targets' initial positions. The measurement sampling time interval is 1 second and the simulation contains 20 seconds. At each sampling time instant, all the sensors measure the two targets and EKF works. The fixed shared sensor locates at $(200, -100)$m. During the tracking process, the non-shared sensors will move to keep the sensor-target geometries always being optimal using the proposed method in Table V. As a comparison, in another situation, the non-shared sensors move randomly from different initial positions. The detailed sensor-target geometries and mean-squared-error from 1000 Monte Carlo repeats of the two situations are provided in Fig. 12. The performance of the situation using the real-time optimized sensor-target geometries is better than the other one. The proposed method

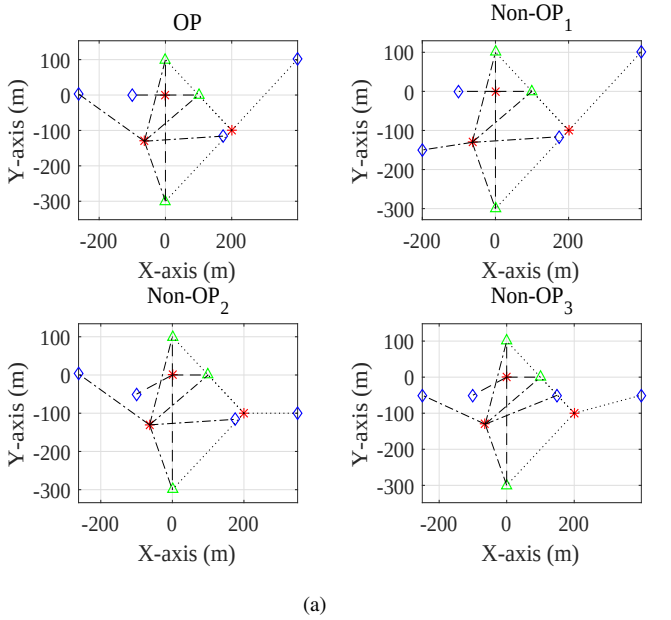


(a)

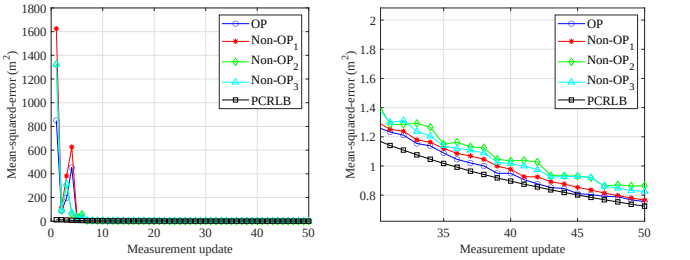


(b) (c)

Fig. 7. EKF results of example 2, (a) different geometries, (b) performance (c) zoom view.



(a)



(b) (c)

Fig. 8. EKF results of example 3, (a) different geometries, (b) performance (c) zoom view.

in Section V.B is effective for mobile target tracking.

For example 6, we assume $M = 1$, $N_1 = 1$ and $N_2 = 1$ (total 3 sensors) to localize $K = 2$ targets. The two statistic targets locate at $(0, 0)$m and $(300, 0)$m. Data association exists in the shared sensor (located at $200, -100$m). We use the proposed extended method in Table VI. Subsequently, the non-shared sensors move randomly and obtain 5 measurements (which can be increased to help solve the data association). Meanwhile, we use EKF to estimate the targets' positions which are shown in Fig. 13(a). Then, we compare the estimated target positions and the measurements of the shared sensor, to obtain the relation between the measurements and target indices. This step is shown in Fig. 13(b). Finally, we just need to follow Steps 4 and 5 in Table VI to optimize the localization performance. Last but not least, if the distances between the shared sensors and different targets are uniform, the data association will have a limited impact on the estimation. Thus, it may be not necessary to resolve data association in this situation because the shared sensors' measurements of different targets are similar.

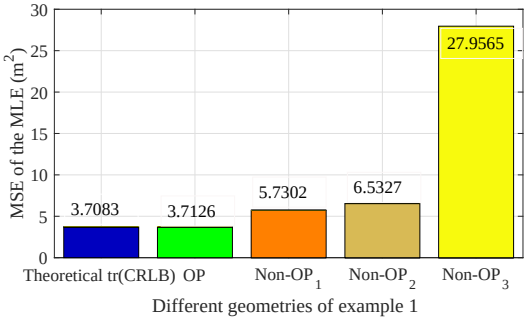


Fig. 9. MLE results of example 1.

VII. Conclusion and Discussion

In this paper, we have proposed a hybrid optimal TOA sensor placement method to acquire the minimum trace of the inverse FIM i.e. tr(CRLB), for multi-target localization. The optimization model considering shared sensors for simultaneous localization of multiple targets is firstly formulated. Secondly, systematic theoretical results for the optimal sensor placement are found. The analytical approaches are based on rigorous geometrical derivations. They provide optimal conditions for many cases and even closed form solutions for

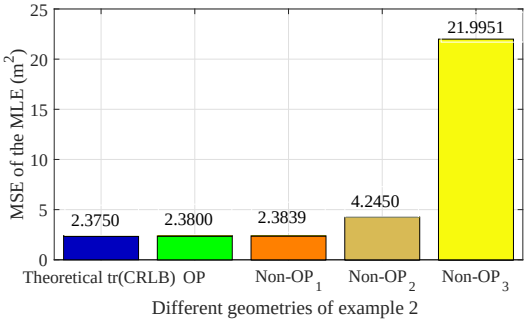


Fig. 10. MLE results of example 2.

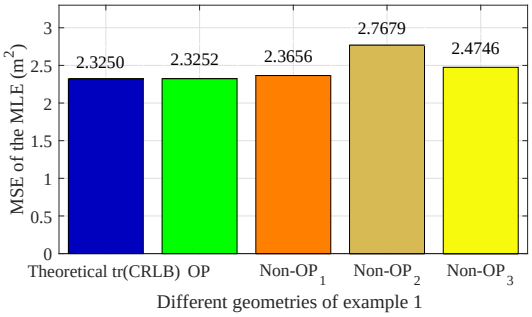


Fig. 11. MLE results of example 3.

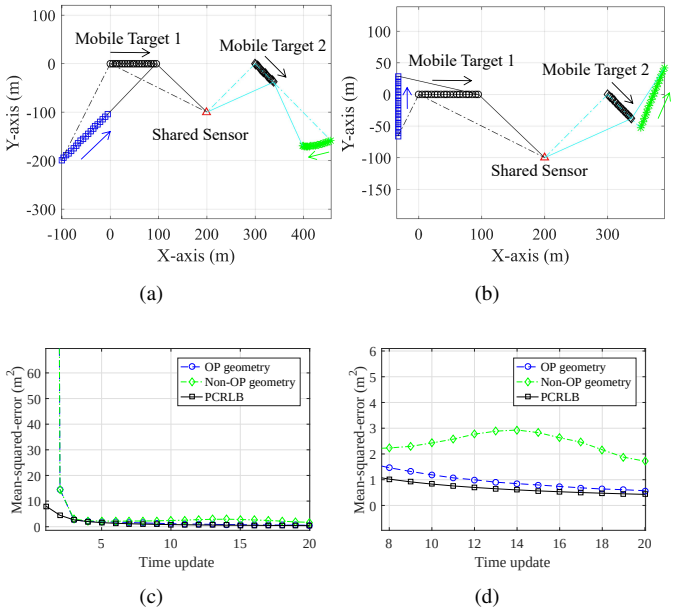


Fig. 12. Results of example 5, (a) the dynamical optimal geometries, (b) the dynamical non-optimal geometries, (c) (d) estimation performance with zoom view.

some special cases. The reachable optimal tr(CRLB) is also derived. However, when the model becomes complicated with more practical constraints, this approach is usually hard to conduct due to intractable mathematical expressions. Thirdly, a novel algebraic optimization algorithm to quickly find the optimal placement is explored. This optimization approach can provide a numerical sub-optimal solution. Fourthly, we

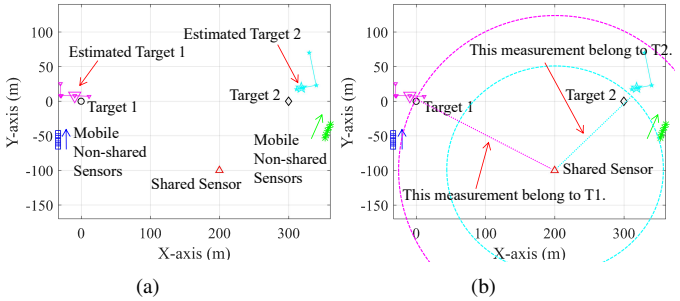


Fig. 13. Results of example 6, (a) estimate the rough targets' positions using mobile non-shared sensors, (b) matching the shared sensors' measurements and estimated targets.

propose a hybrid method for solving the most general situation, including both the theoretical and mathematical solutions. Finally, the simulation studies provide sufficient examples to verify the correctness and effectiveness of both the proposed theoretical and mathematical methods.

In practical implementations, the unknown target location is replaced by an initial estimate to calculate an optimal sensor placement. Iterating this estimation-optimal placement process eventually leads to an optimal localization and placement result. In addition, the proposed method allows evaluation of the estimation performance based on the acquired accuracy lower bound. The disadvantages of only using non-shared sensors (e.g., low effectiveness and requiring a lot of sensors) and the limitations of only using shared sensors (e.g., high equipment cost and unsatisfactory flexibility) are improved by the proposed method. The first proposed numerical optimization algorithm is an improvement over search-based methods and resolves the convergence problem properly. Furthermore, the proposed hybrid method can quickly and definitely find a (sub-)optimal solution for different situations. In future work, the case of freely placed (mobile) shared sensors will be explored. In this case, both the theoretical and numerical optimization will become more complicated since the constraints used to simplify the objective function will not hold. Furthermore, the optimal results of this paper can be extended into the 3D space in the future.

VIII. Appendix A

The derivation of the CRLB is provided.

Since all sensor measurement noises are white Gaussian random variables (some sensors are allowed to have different noise variances), and thus the joint probability density function (PDF) of all sensor measurements is multidimensional Gaussian given by the product of individual sensor measurement PDFs [12]. Therefore the log-likelihood takes the form

$$p(\tilde{\boldsymbol{s}};\boldsymbol{p}) = \frac{1}{(2\pi)^{\frac{W}{2}}\left(\det \boldsymbol{\Sigma}_0\right)^{\frac{1}{2}}} \exp\left\{-\frac{1}{2}\left[\tilde{\boldsymbol{s}}-\boldsymbol{g}(\boldsymbol{p})\right]^T \boldsymbol{\Sigma}_0^{-1}\left[\tilde{\boldsymbol{s}}-\boldsymbol{g}(\boldsymbol{p})\right]\right\}, \tag{35}$$

where W denotes the total measurements of both the non-shared and shared sensors from different targets, and based on the definitions in this paper, $W = N_1+N_2...+N+KM$ (more

specifically, $N_1 + N_2 ... + N_K$ non-shared sensors' measurements, M shared sensors and each one has K measurements). Also, we define $w = 1, 2, ...W$, and $g_w(\cdot)$ denotes the function between the true targets and the wth measurement. Then, when the measurement noise is Gaussian white and the measurement noise variance σ_{ik}^2 is independent with the target positions, the FIM takes the form

$$\boldsymbol{\Phi} = E\left[\left(\frac{\partial \ln p(\tilde{\boldsymbol{s}};\boldsymbol{p})}{\partial \boldsymbol{p}}\right)\left(\frac{\partial \ln p(\tilde{\boldsymbol{s}};\boldsymbol{p})}{\partial \boldsymbol{p}}\right)^T\right] = \boldsymbol{J}_o^T \boldsymbol{\Sigma}_o^{-1} \boldsymbol{J}_o. \tag{36}$$

Please note that the very detailed derivation in (36) has already been provided in book [12], i.e., pages 73-76 of Chapter 3 Appendix 3C "Derivation of General Gaussian CRLB". We obtain

$$\boldsymbol{\Phi} = \boldsymbol{J}_o^T \boldsymbol{\Sigma}_o^{-1} \boldsymbol{J}_o, \tag{37}$$

where $\boldsymbol{J}_o$ and $\boldsymbol{\Sigma}_0$ are defined as (7). Next, to acquire the full expression of the FIM, we need to calculate $\boldsymbol{J}_{ik}$ which is the partial derivative evaluated at the true target k. We have

$$\boldsymbol{J}_{ik} = \left[\ \cdots,\ \ \frac{\partial \tilde{s}_{ik}}{\partial p_{xk}},\ \ \frac{\partial \tilde{s}_{ik}}{\partial p_{yk}},\ \ \cdots\ \right], \tag{38}$$

and then the entries in (38) are calculated by

$$\begin{aligned}\frac{\partial \tilde{s}_{ik}}{\partial p_{xk}} &= \frac{\partial 2\sqrt{(p_{xk}-r_{xi})^2+(p_{yk}-r_{yi})^2}}{\partial p_{xk}} \\ &= \frac{2(p_x - r_{xi})}{d_{ik}} = 2\cos\theta_{ik},\end{aligned} \tag{39}$$

$$\begin{aligned}\frac{\partial \tilde{s}_{ik}}{\partial p_{yk}} &= \frac{\partial 2\sqrt{(p_{xk}-r_{xi})^2+(p_{yk}-r_{yi})^2}}{\partial p_{yk}} \\ &= \frac{2(p_{yk} - r_{yi})}{d_{ik}} = 2\sin\theta_{ik}.\end{aligned} \tag{40}$$

Then, we obtain the final expression of the FIM as shown in (12). Finally, the CRLB matrix has CRLB=$\boldsymbol{\Phi}^{-1}$.

IX. Appendix B

The regularity condition of unbiasedness of the estimator is proven.

In (35) of Appendix A, the PDF of all the measurements are derived. Then, we have

$$\begin{aligned}&\frac{\partial \ln p(\tilde{\boldsymbol{s}};\boldsymbol{p})}{\partial \boldsymbol{p}} \\ =&\frac{\partial}{\partial \boldsymbol{p}}\left\{\ln \frac{1}{(2\pi)^{\frac{W}{2}}(\det \boldsymbol{\Sigma}_0)^{\frac{1}{2}}}\right. \\ &\left.-\frac{1}{2}\sum_{w=1}^{W}\left[\tilde{s}_w - g_w(\boldsymbol{p})\right]\sigma_w^{-2}\left[\tilde{s}_w - g_w(\boldsymbol{p})\right]\right\} \\ =&\frac{\partial -\frac{1}{2}\sum_{w=1}^{W}\left[\tilde{s}_w - g_w(\boldsymbol{p})\right]\sigma_w^{-2}\left[\tilde{s}_w - g_w(\boldsymbol{p})\right]}{\partial \boldsymbol{p}} \\ =&\sum_{w=1}^{W}\frac{1}{\sigma_w^{-2}}\left[\tilde{s}_w - g_w(\boldsymbol{p})\right]\frac{\partial g_w(\boldsymbol{p})}{\partial \boldsymbol{p}} \\ =&\sum_{w=1}^{W}\frac{1}{\sigma_w^{-2}}\left[\tilde{s}_w\frac{\partial g_w(\boldsymbol{p})}{\partial \boldsymbol{p}} - g_w(\boldsymbol{p})\frac{\partial g_w(\boldsymbol{p})}{\partial \boldsymbol{p}}\right].\end{aligned} \tag{41}$$

Combining (35) with the measurement model in the manuscript, i.e., $\tilde{s}_w = g_w(\boldsymbol{p}) + c\eta_w$, we have $c\eta_w \sim \mathcal{N}\left(0, \sigma_w^2\right)$. The other variables contain no random noise. The expectation of (35) is

$$\begin{aligned}&E\left\{\sum_{w=1}^{W}\frac{1}{\sigma_w^{-2}}\left[\tilde{s}_w\frac{\partial g_w(\boldsymbol{p})}{\partial \boldsymbol{p}} - g_w(\boldsymbol{p})\frac{\partial g_w(\boldsymbol{p})}{\partial \boldsymbol{p}}\right]\right\} \\ =&\sum_{w=1}^{W}\frac{1}{\sigma_w^{-2}}\left\{E\left[\tilde{s}_w\frac{\partial g_w(\boldsymbol{p})}{\partial \boldsymbol{p}}\right] - E\left[g_w(\boldsymbol{p})\frac{\partial g_w(\boldsymbol{p})}{\partial \boldsymbol{p}}\right]\right\} \\ =&\sum_{w=1}^{W}\frac{1}{\sigma_w^{-2}}\left\{E\left[g_w(\boldsymbol{p})\frac{\partial g_w(\boldsymbol{p})}{\partial \boldsymbol{p}}\right] + E\left[c\eta_w\frac{\partial g_w(\boldsymbol{p})}{\partial \boldsymbol{p}}\right]\right. \\ &\left.-E\left[g_w(\boldsymbol{p})\frac{\partial g_w(\boldsymbol{p})}{\partial \boldsymbol{p}}\right]\right\}.\end{aligned} \tag{42}$$

Since $c\eta_w$ is independent of $\frac{\partial g_w(\boldsymbol{p})}{\partial \boldsymbol{p}}$, we have

$$E\left[c\eta_w\frac{\partial g_w(\boldsymbol{p})}{\partial \boldsymbol{p}}\right] = E\left[c\eta_w\right]\cdot E\left[\frac{\partial g_w(\boldsymbol{p})}{\partial \boldsymbol{p}}\right] = 0. \tag{43}$$

Thus, substituting (43) back to (42), we obtain $\frac{\partial \ln p(\tilde{\boldsymbol{s}};\boldsymbol{p})}{\partial \boldsymbol{p}} = 0$, and the regularity condition is satisfied.

Since the regularity condition is always held, the unbiasedness of a well-selected estimator is guaranteed. Note that the different measurement noise variances of using non-uniform sensors will not impact the regularity condition.

X. Appendix C

The derivation of the posterior CRLB (PCRLB) is provided.

For the iterative estimation methods, e.g., EKF, the PCRLB is a commonly used benchmark to evaluate the realtime performance. Firstly, some definitions are needed, and for each target estimation, one estimator (i.e., EKF) is required. Thus, K EKFs are required and they are independent. For simplification reasons, the subscript k to denote the target index is ignored. We define the state in the kth EKF as

$$\begin{aligned}&\boldsymbol{x}_{\kappa|\kappa} = [\boldsymbol{p}_{x\kappa}; \boldsymbol{p}_{y\kappa}; \dot{\boldsymbol{p}}_{x\kappa}; \dot{\boldsymbol{p}}_{y\kappa}], \\ \text{and}\quad &\boldsymbol{x}_{\kappa+1} = \boldsymbol{F}\boldsymbol{x}_{\kappa} + \boldsymbol{w}_{\kappa}\end{aligned} \tag{44}$$

where κ denotes the measurement update index, $\dot{\boldsymbol{p}}_{x\kappa}, \dot{\boldsymbol{p}}_{y\kappa}$ are the target velocities and $\boldsymbol{w}_{\kappa} \sim (0, \boldsymbol{Q})$ is the zero-mean Gaussian independent process noise. Besides, Δt is the sampling time interval and we have

$$\begin{aligned}\boldsymbol{F} &= \begin{bmatrix} 1 & 0 & \Delta t & 0 \\ 0 & 1 & 0 & \Delta t \\ 0 & 0 & 1 & 0 \\ 0 & 0 & 0 & 1 \end{bmatrix}, \quad \text{and} \\ \boldsymbol{Q} &= \begin{bmatrix} q^x\frac{\Delta t^3}{3} & 0 & q^x\frac{\Delta t^2}{2} & 0 \\ 0 & q^y\frac{\Delta t^3}{3} & 0 & q^y\frac{\Delta t^2}{2} \\ q^x\frac{\Delta t^2}{2} & 0 & q^x\Delta t & 0 \\ 0 & q^y\frac{\Delta t^2}{2} & 0 & q^y\Delta t \end{bmatrix}.\end{aligned} \tag{45}$$

The EKF algorithm is

$$\boldsymbol{x}_{\kappa+1|\kappa} = \boldsymbol{F}\boldsymbol{x}_{\kappa|\kappa} \tag{46a}$$

$$\boldsymbol{P}_{\kappa+1|\kappa} = \boldsymbol{F}\boldsymbol{P}_{\kappa|\kappa}\boldsymbol{F}^T + \boldsymbol{Q} \tag{46b}$$

$$\boldsymbol{K}_{\kappa+1} = \boldsymbol{P}_{\kappa+1|\kappa}\boldsymbol{H}_{\kappa+1}^T(R_k + \boldsymbol{H}_{\kappa+1}\boldsymbol{P}_{\kappa+1|\kappa}\boldsymbol{H}_{\kappa+1}^T)^{-1} \tag{46c}$$

$$\boldsymbol{x}_{\kappa+1|\kappa+1} = \boldsymbol{x}_{\kappa+1|\kappa} + \boldsymbol{K}_{\kappa+1}(\tilde{\boldsymbol{z}}_{\kappa+1} - \boldsymbol{H}_{\kappa+1}\boldsymbol{x}_{\kappa+1|\kappa}) \tag{46d}$$

$$\boldsymbol{P}_{\kappa+1|\kappa+1} = \boldsymbol{P}_{\kappa+1|\kappa} - \boldsymbol{K}_{\kappa+1}\boldsymbol{H}_{\kappa+1}\boldsymbol{P}_{\kappa+1|\kappa} \tag{46e}$$

where $\boldsymbol{H}_{\kappa+1}$ is the Jacobian matrix of measurement model (3) respect to the priori estimate $\boldsymbol{x}_{\kappa+1|\kappa}$ because the true $\boldsymbol{x}_{\kappa+1}$ is unknown. R_κ is the measurement vriance.

According to [49] [47], a classical way to compute the recursive FIM, $\boldsymbol{\Psi}_\kappa$, which is the inverse of the PCRLB, is

$$\boldsymbol{\Psi}_{\kappa+1} = -\boldsymbol{D}_\kappa^{(3)}(\boldsymbol{\Psi}_\kappa + \boldsymbol{D}_\kappa^{(1)})^{-1}\boldsymbol{D}_\kappa^{(2)} + \boldsymbol{D}_\kappa^{(4)} \tag{47}$$

where

$$\begin{aligned}
\boldsymbol{D}_\kappa^{(1)} =& E\left[-\Delta_{\boldsymbol{x}_\kappa}^{\boldsymbol{x}_\kappa}\ln p(\boldsymbol{x}_{\kappa+1|\kappa})\right]\\
\boldsymbol{D}_\kappa^{(2)} =& E\left[-\Delta_{\boldsymbol{x}_\kappa}^{\boldsymbol{x}_{\kappa+1}}\ln p(\boldsymbol{x}_{\kappa+1|\kappa})\right]\\
\boldsymbol{D}_\kappa^{(3)} =& E\left[-\Delta_{\boldsymbol{x}_{\kappa+1}}^{\boldsymbol{x}_\kappa}\ln p(\boldsymbol{x}_{\kappa+1|\kappa})\right]\\
\boldsymbol{D}_\kappa^{(4)} =& E\left[-\Delta_{\boldsymbol{x}_{\kappa+1}}^{\boldsymbol{x}_{\kappa+1}}\ln p(\boldsymbol{x}_{\kappa+1|\kappa})\right]\\
&+ E\left[-\Delta_{\boldsymbol{x}_{\kappa+1}}^{\boldsymbol{x}_{\kappa+1}}\ln p(\tilde{s}_{\kappa+1}|\boldsymbol{x}_{\kappa+1})\right].
\end{aligned} \tag{48}$$

$p(\boldsymbol{x}_{\kappa+1|\kappa})$ and $p(\tilde{s}_{\kappa+1}|\boldsymbol{x}_{\kappa+1})$ are the dynamic transition and observation PDFs of the equations (44) and (3). Compared with the work in [47], the only difference in this paper is that the measurement model is TOA rather than AOA. Subsequently, we have

$$\begin{aligned}
\boldsymbol{D}_\kappa^{(1)} =& \boldsymbol{F}^T\boldsymbol{Q}^{-1}\boldsymbol{F},\\
\boldsymbol{D}_\kappa^{(2)} =& -\boldsymbol{F}^T\boldsymbol{Q}^{-1},\\
\boldsymbol{D}_\kappa^{(3)} =& -\boldsymbol{Q}^{-1}\boldsymbol{F}\\
\boldsymbol{D}_\kappa^{(4)} =& \boldsymbol{Q}^{-1} + \frac{1}{\sigma_\kappa^2}E[\boldsymbol{V}_{\boldsymbol{\kappa}}^T\boldsymbol{V}_{\boldsymbol{\kappa}}],
\end{aligned} \tag{49}$$

where σ_κ^2 denotes the sensor noise variance of the κth measurement, and

$$\begin{aligned}
\boldsymbol{V}_{\boldsymbol{\kappa}} &= \left[\frac{s_\kappa}{\partial \boldsymbol{p}_{x\kappa}}, \frac{s_\kappa}{\partial \boldsymbol{p}_{y\kappa}}, \frac{s_\kappa}{\partial \dot{\boldsymbol{p}}_{x\kappa}}, \frac{s_\kappa}{\partial \dot{\boldsymbol{p}}_{y\kappa}}\right]\\
&= \left[2\cos\theta_\kappa, 2\sin\theta_\kappa, 0, 0\right].
\end{aligned} \tag{50}$$

Substituting (49) back to (47) and the inverse of the PCRLB becomes

$$\begin{aligned}
\boldsymbol{\Psi}_{\kappa+1} =& -\boldsymbol{Q}^{-1}\boldsymbol{F}(\boldsymbol{\Psi}_\kappa + \boldsymbol{F}^T\boldsymbol{Q}^{-1}\boldsymbol{F})^{-1}\boldsymbol{F}^T\boldsymbol{Q}^{-1}\\
&+ \boldsymbol{Q}^{-1} + \frac{1}{\sigma_\kappa^2}E[\boldsymbol{V}_{\boldsymbol{\kappa}}^T\boldsymbol{V}_{\boldsymbol{\kappa}}],
\end{aligned} \tag{51}$$

which can be written as

$$\boldsymbol{\Psi}_{\kappa+1} = (\boldsymbol{Q} + \boldsymbol{F}\boldsymbol{\Psi}_\kappa^{-1}\boldsymbol{F}^T)^{-1} + \frac{1}{\sigma_\kappa^2}E[\boldsymbol{V}_{\boldsymbol{\kappa}}^T\boldsymbol{V}_{\boldsymbol{\kappa}}], \tag{52}$$

and finally $\text{PCRLB}_{\kappa+1} = \boldsymbol{\Psi}_{\kappa+1}^{-1}$. The initial of $\boldsymbol{\Psi}_0$ can be an eye matrix or set by the initial measurements, i.e., $\frac{1}{\sigma_0^2}E[\boldsymbol{V}_{\boldsymbol{0}}^T\boldsymbol{V}_{\boldsymbol{0}}]$. Note that Monte Carlo repeats of the EKF are required to calculate the PCRLB because of the expectation calculation $E[\cdot]$.

REFERENCES

[1] M. Z. Win, Y. Shen, and W. Dai, "A theoretical foundation of network localization and navigation," *Proceedings of the IEEE*, vol. 106, no. 7, pp. 1136–1165, 2018.

[2] M. Chiani, A. Giorgetti, and E. Paolini, "Sensor radar for object tracking," *Proceedings of the IEEE*, vol. 106, no. 6, pp. 1022–1041, 2018.

[3] A. Conti, S. Mazuelas, S. Bartoletti, W. C. Lindsey, and M. Z. Win, "Soft information for localization-of-things," *Proceedings of the IEEE*, vol. 107, no. 11, pp. 2240–2264, 2019.

[4] S. Xu, J. Liu, C. Yang, X. Wu, and T. Xu, "A learning-based stable servo control strategy using broad learning system applied for microrobotic control," *IEEE Transactions on Cybernetics*, pp. 1–11, 2021, DOI:10.1109/TCYB.2021.3121080.

[5] A. N. Bishop, B. Fidan, B. Anderson, K. Doğançay, and P. N. Pathirana, "Optimality analysis of sensor-target localization geometries," *Automatica*, vol. 46, no. 3, pp. 479–492, 2010.

[6] N. H. Nguyen and K. Doğançay, "Optimal geometry analysis for multistatic TOA localization," *IEEE Transactions on Signal Processing*, vol. 64, no. 16, pp. 4180–4193, 2016.

[7] X. R. Li, "RSS-based location estimation with unknown pathloss model," *IEEE Transactions on Wireless Communications*, vol. 5, no. 12, pp. 3626–3633, 2006.

[8] H. C. So, "Source localization: Algorithms and analysis," *Handbook of Position Location: Theory, Practice, and Advances*, pp. 25–66, 2011.

[9] S. Chen and K. C. Ho, "Achieving asymptotic efficient performance for squared range and squared range difference localizations," *IEEE Transactions on Signal Processing*, vol. 61, no. 11, pp. 2836–2849, 2013.

[10] A. Beck, P. Stoica, and J. Li, "Exact and approximate solutions of source localization problems," *IEEE Transactions on Signal Processing*, vol. 56, no. 5, pp. 1770–1778, 2008.

[11] V. J. Aidala, "Kalman filter behavior in bearings-only tracking applications," *IEEE Transactions on Aerospace and Electronic Systems*, vol. AES-15, no. 1, pp. 29–39, Jan 1979.

[12] S. M. Kay, *Fundamentals of Statistical Signal Processing: Estimation Theory*. Englewood Cliffs, NJ: Prentice-Hall, 1993.

[13] K. Doğançay, "Bias compensation for the bearings-only pseudolinear target track estimator," *IEEE Transactions on Signal Processing*, vol. 54, no. 1, pp. 59–68, 2006.

[14] S. Xu, K. Doğançay, and H. Hmam, "Distributed pseudolinear estimation and UAV path optimization for 3D AOA target tracking," *Signal Processing*, vol. 133, pp. 64–78, 2017.

[15] S. C. Nardone, A. G. Lindgren, and K. F. Gong, "Fundamental properties and performance of conventional bearings-only target motion analysis," *IEEE Transactions on Automatic Control*, vol. 29, no. 9, pp. 775–787, 1984.

[16] M. S. Arulampalam, S. Maskell, N. Gordon, and T. Clapp, "A tutorial on particle filters for online nonlinear/non-gaussian bayesian tracking," *IEEE Transactions on Signal Processing*, vol. 50, no. 2, pp. 174–188, 2002.

[17] J. A. Fawcett, "Effect of course maneuvers on bearings-only range estimation," *IEEE Transactions on Acoustics, Speech and Signal Processing*, vol. 36, no. 8, pp. 1193–1199, 1988.

[18] Y. Oshman and P. Davidson, "Optimization of observer trajectories for bearings-only target localization," *IEEE Transactions on Aerospace and Electronic Systems*, vol. 35, no. 3, pp. 892–902, 1999.

[19] S. Xu, Y. Ou, and X. Wu, "Optimal sensor placement for 3-D time-of-arrival target localization," *IEEE Transactions on Signal Processing*, vol. 67, no. 19, pp. 5018–5031, 2019.

[20] D. Moreno-Salinas, A. Pascoal, and J. Aranda, "Optimal sensor placement for acoustic underwater target positioning with range-only measurements," *IEEE Journal of Oceanic Engineering*, vol. 41, no. 3, pp. 620–643, 2016.

[21] D. Ucinski, *Optimal measurement methods for distributed parameter system identification*. Boca Raton, Florida, U.S., CRC Press, 2005.

[22] S. Zhao, B. Chen, and T. H. Lee, "Optimal sensor placement for target localization and tracking in 2D and 3D," *International Journal of Control*, vol. 86, no. 10, pp. 1687–1704, 2013.

[23] L. Rui and K. C. Ho, "Elliptic localization: Performance study and optimum receiver placement," *IEEE Transactions on Signal Processing*, vol. 62, no. 18, pp. 4673–4688, 2014.

[24] S. Xu and K. Doğançay, "Optimal sensor placement for 3-

D angle-of-arrival target localization," *IEEE Transactions on Aerospace and Electronic Systems*, vol. 53, no. 3, pp. 1196–1211, 2017.

[25] D. Moreno-Salinas, A. M. Pascoal, and J. Aranda, "Optimal sensor placement for multiple target positioning with range-only measurements in two-dimensional scenarios," *Sensors*, vol. 13, no. 8, pp. 10 674–10 710, 2013.

[26] Y. Li, G. Qi, and A. Sheng, "Optimal deployment of vehicles with circular formation for bearings-only multi-target localization," *Automatica*, vol. 105, pp. 347 – 355, 2019.

[27] A. M. Aziz, "A novel all-neighbor fuzzy association approach for multitarget tracking in a cluttered environment," *Signal Processing*, vol. 91, no. 8, pp. 2001–2015, 2011.

[28] Y. Bar-Shalom, "Multitarget-multisensor tracking: Applications and advances. volume III," *Norwood, MA, Artech House, Inc.*, 2000.

[29] S. S. Blackman, "Multiple hypothesis tracking for multiple target tracking," *IEEE Aerospace and Electronic Systems Magazine*, vol. 19, no. 1, pp. 5–18, 2004.

[30] T. E. Fortmann, Y. Bar-Shalom, and M. Scheffe, "Sonar tracking of multiple targets using joint probabilistic data association," *IEEE Journal of Oceanic Engineering*, vol. 8, no. 3, pp. 173–184, 1983.

[31] S. Blackrnan and A. House, "Design and analysis of modern tracking systems," *Boston, MA: Artech House*, 1999.

[32] S. Xu, M. Rice, and F. Rice, "Optimal toa-sensor placement for two target localization simultaneously using shared sensors," *IEEE Communications Letters*, vol. 25, no. 8, pp. 2584–2588, 2021.

[33] Y. Zhao, R. Schwartz, E. Salomons, A. Ostfeld, and H. V. Poor, "New formulation and optimization methods for water sensor placement," *Environmental Modelling & Software*, vol. 76, pp. 128–136, 2016.

[34] C. Jiang, Y. Soh, and H. Li, "Sensor placement by maximal projection on minimum eigenspace for linear inverse problems," *IEEE Transactions on Signal Processing*, vol. 64, no. 21, pp. 5595–5610, 2016.

[35] C. Jiang, Z. Chen, R. Su, and Y. Soh, "Group greedy method for sensor placement," *IEEE Transactions on Signal Processing*, vol. 67, no. 9, pp. 2249–2262, 2019.

[36] S. P. Chepuri and G. Leus, "Continuous sensor placement," *IEEE Signal Processing Letters*, vol. 22, no. 5, pp. 544–548, 2014.

[37] N. Sahu, L. Wu, P. Babu, B. Shankar M. R., and B. Ottersten, "Optimal sensor placement for source localization: A unified ADMM approach," *IEEE Transactions on Vehicular Technology*, pp. 1–13, 2022, DOI:10.1109/TVT.2022.3146603.

[38] S. Coraluppi and C. Carthel, "Distributed tracking in multistatic sonar," *IEEE Transactions on Aerospace and Electronic Systems*, vol. 41, no. 3, pp. 1138–1147, 2005.

[39] A. Munaf, G. Canepa, and K. D. LePage, "Continuous active sonars for littoral undersea surveillance," *IEEE Journal of Oceanic Engineering*, vol. 44, no. 4, pp. 1198–1212, 2019.

[40] M. Chiani, A. Giorgetti, and E. Paolini, "Sensor radar for object tracking," *Proceedings of the IEEE*, vol. 106, no. 6, pp. 1022–1041, 2018.

[41] S. Xu, "Optimal sensor placement for target localization using hybrid RSS, AOA and TOA measurements," *IEEE Communications Letters*, vol. 24, no. 9, pp. 1966–1970, 2020.

[42] D. J. Torrieri, "Statistical theory of passive location systems," *IEEE Transactions on Aerospace and Electronic Systems*, vol. AES-20, no. 2, pp. 183–198, 1984.

[43] D. Moreno-Salinas, A. Pascoal, and J. Aranda, "Sensor networks for optimal target localization with bearings-only measurements in constrained three-dimensional scenarios," *Sensors*, vol. 13, no. 8, pp. 10 386–10 417, 2013.

[44] S. Xu and K. Doğançay, "Optimal sensor deployment for 3D AOA target localization," in *IEEE International Conference on Acoustics, Speech and Signal Processing (ICASSP)*, April 2015, pp. 2544–2548.

[45] J. M. Danskin, "The theory of max-min, with applications," *SIAM Journal on Applied Mathematics*, vol. 14, no. 4, pp. 641–664, 1966.

[46] C. Jin, P. Netrapalli, and M. Jordan, "What is local optimality in nonconvex-nonconcave minimax optimization?" in *International Conference on Machine Learning*. PMLR, 2020, pp. 4880–4889.

[47] N. H. Nguyen and K. Doğançay, "Improved pseudolinear kalman filter algorithms for bearings-only target tracking," *IEEE Transactions on Signal Processing*, vol. 65, no. 23, pp. 6119–6134, 2017.

[48] K. Doğançay and G. Ibal, "Instrumental variable estimator for 3D bearings-only emitter localization," in *International Conference on Intelligent Sensors, Sensor Networks and Information Processing*, 2005, pp. 63–68.

[49] P. Tichavsky, C. H. Muravchik, and A. Nehorai, "Posterior Cramér-Rao bounds for discrete-time nonlinear filtering," *IEEE Transactions on Signal Processing*, vol. 46, no. 5, pp. 1386–1396, 1998.